Chapter 8
Failure Theories of Piezoelectric Materials

Abstract In this chapter failure experiments and theories in piezoelectric materials are discussed. In present time the precision of experiments should still be improved. The failure theory in solids is very complicated and there is no unified critical criterion. It is clear that the critical energy for different failure version is different. Especially the version of brittle tension failure is significantly different with other versions. In piezoelectric ceramics the failure energy density of an electric field is much higher than that in mechanical loading. In this chapter the generalized stress intensity factor criterions; total, mechanical, and local energy release rate criterions; strain energy density factor criterion; modal strain energy density factor theory; small-scale domain switching theory; failure criterion of conductive cracks with charge-free zone model are studied. Some simple electric breakdown theories of solid dielectrics are also discussed.

Keywords Failure theories • Generalized stress intensity factor • Energy release rate • Modal strain energy • Charge-free zone model • Electric breakdown

8.1 Experimental Studies

The change of the microstructure, including plastic yielding, phase transformation, and failure theory, in solids is very complicated, and in present time there is no unified critical criterion to show these changes exactly. In general the change of the internal microstructure in the materials is caused by deformation, electromagnetic field and temperature. Experiments show that except the failure under tension, before failure the continuous deformation is revealed and then follows the change of the microstructure, so the failure and plastic yielding, etc. often posses the similar criterion. However, the failure of a brittle material under tension is less connected to the continuous deformation, so it should often be discussed in different theory. The experiments are necessary to get the practical failure criterions in engineering. Many experiments for failure have been carried out. Because the piezoelectric specimens are thin and small, manufacturing an ideal crack is very difficult. Usually the crack

Z.-B. Kuang, *Theory of Electroelasticity*, DOI 10.1007/978-3-642-36291-0_8,

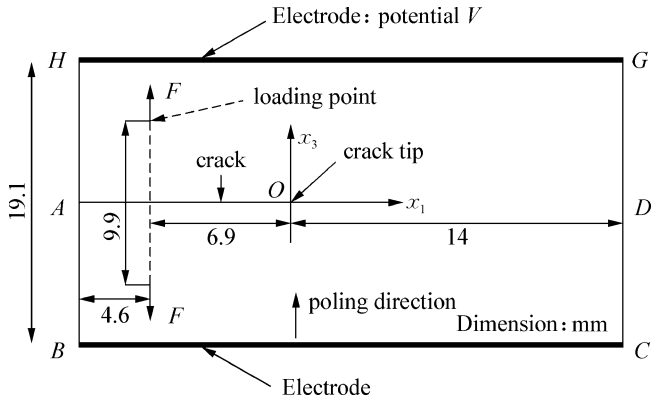

Fig. 8.1 Compact tension (*CT*) specimen

is a narrow slit with a circular end. The precision of the experimental results is not very well, and the experiments are needed in the future. The fatigue failure is not discussed in this book.

8.1.1 Test on Compact Tension Specimens

Park and Sun (1995) carried out the mode-I fracture tests of the compact tension (CT) specimen for PZT-4 ceramic. Two silver-coated faces at the upper and lower surfaces of the sample were used as electrodes. The sizes of the specimen are $25.5 \times 19.1 \times 5.1\,\text{mm}^3$ with crack length 11.5 mm as shown in Fig. 8.1. The polarization x_3-axis is perpendicular to the crack. The crack was created by cutting with a 0.46 mm thick diamond wheel and further cut by a sharp razor blade with diamond abrasive. Because the electric field exceeded $5\,\text{Kv/m}$ the electric discharging between electrodes through the air was observed, the specimen was immersed in a tube filled with silicone oil. The tests were to increase the tensile load until failure occurred under a certain electric field. Some experimental results can be found in Fig. 8.13. The results showed that the positive electric fields enforce the crack propagation or decrease the apparent fracture toughness K_{Ic}, while negative electric field impede crack propagation or increase the apparent fracture toughness.

Fang et al. (2004) carried out the tensile tests of the plate specimen with a central crack for PZT-5 ceramic. The sizes of the specimen are $40 \times 20 \times 3\,\text{mm}^3$ with the polarization x_3-axis. Their results are similar to that of Park and Sun.

8.1.2 Three-Point Bending Test with Asymmetric Crack

Park and Sun (1995) carried out the mixed-mode fracture tests on the three-point bend specimen with unsymmetrical crack for PZT-4 ceramic. The sizes of the specimen are $19.1 \times 9 \times 5.1\,\text{mm}^3$, and the poling direction was perpendicular to

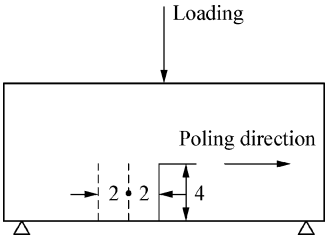

Fig. 8.2 Specimen for mixed-mode fracture test

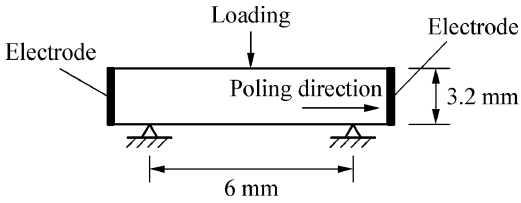

Fig. 8.3 Three-point smooth bending test specimen

the crack as shown in Fig. 8.2. The length of the crack is 4.0 mm and located at the midspan, 2 mm, 4 mm from the midspan, respectively. The center-cracked specimens produced mode-I fracture, and other two kinds of specimens exhibited mixed-mode fracture. The experimental results showed that the fracture in this test exhibits the same behaviors as that in CT specimens. It is also shown that the crack deviated from the midspan will increase the fracture load.

8.1.3 Three-Point Bending Test of Smooth Specimens

Fu and Zhang (2000) carried out three-point bending tests of smooth specimens to study the effect of an electric field on bending strength for PZT-841 ceramic (Fig. 8.3). The sizes of the specimen are $10 \times 4 \times 3.2\,\text{mm}^3$ and the span distance was 6.0 mm. The poling direction was perpendicular to the load. Two silver-coated faces at the ends of the sample were used as electrodes. The specimens were thermally depoled at 400 °C for 30 min. Both the loading jig and supports were insulated from the loading system. The generalized stresses will be calculated by the finite element method. Under a mechanical load of 340 N, the electric field was monotonically increased until fracture occurred. The results are shown in Fig. 8.4. Results show that for the depoled specimens, the positive and negative fields all decrease the bending strength.

8.1.4 Test on Conducting Crack

Heyer et al. (1998) carried out the mode-I fracture tests of the four-point bending specimen for PZT-PIC 151 ceramic. Two silver-coated faces at the upper and lower

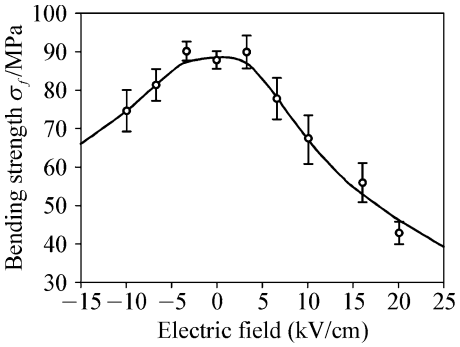

Fig. 8.4 Variations of bending strength with electric field (Reprinted from Fu and Zhang 2000, with permission from *Acta Materialia*)

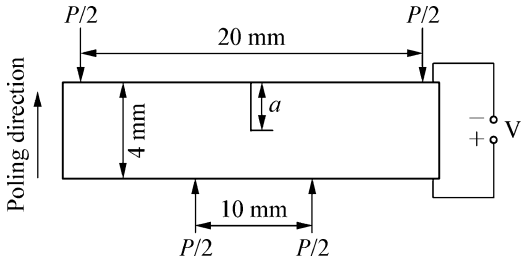

Fig. 8.5 Four-point bending specimen

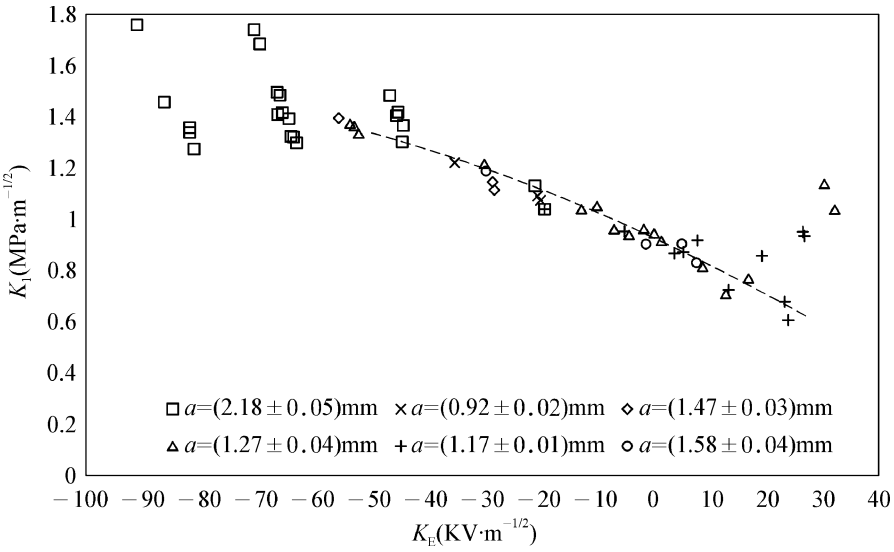

Fig. 8.6 Plot of the stress and electric field intensity factors (Reprinted from Heyer et al. 1998, with permission from *Acta Materialia*)

surfaces of the sample were used as electrodes. The thickness is 3 mm. The crack is filled with NaCl solution and its depth $a = 0.9 \sim 2.2$ mm as shown in Fig. 8.5. The generalized stress intensity factors are calculated by numerical method. The results are shown in Fig. 8.6.

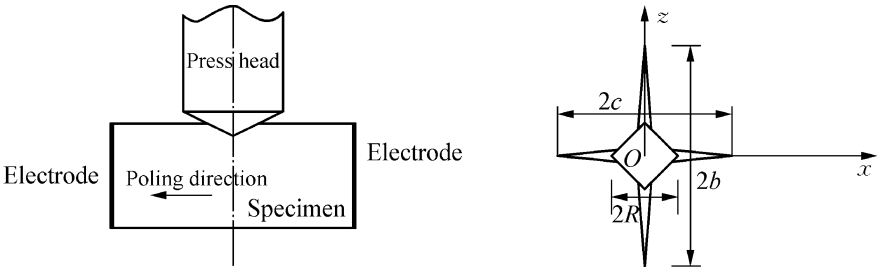

Fig. 8.7 Vicker indentation test

8.1.5 Vicker Indentation Test

The Vicker indentation test technique is pressing a square diamond pyramid into a specimen with a given external force. The resulting wedge force drives radial half penny-shaped cracks. The crack growth version in a Vicker indentation test is quite different with that in the CT test. In the direction perpendicular to the poling direction, the crack length is longer than that in the direction parallel to poling direction (Fig. 8.7). Experiment results (Jiang and Sun 2001) pointed out that for small loading $(9\,\mathrm{N})$, increasing the positive electric field increased the crack and increasing the negative electric field (absolute value) decreased the crack. For a larger loading $(49\,\mathrm{N})$, increasing the positive or negative electric field increased the crack, but in a negative electric field, the crack growth is smaller than that in the positive electric field. In the test of Wang and Singh (1997), the results are somewhat different.

8.2 Some Practical Failure Criterions

8.2.1 Generalized Stress Intensity Factor Criterion

In the linear- and small-scale yielding fracture mechanics for mode-I problem, the stress intensity factor K_I or the energy release rate G or J_I integral is used as the fracture criterion. For mixed fracture problem, the combination of $K_\mathrm{I}, K_\mathrm{II}$ and K_III is used. These theories are successful in engineering, but what combination should be used is still a problem. It is natural to extend these theories to electroelastic fracture problem, i.e., for the mixed fracture problem in piezoelectric material, the fracture criterion takes the following form:

$$f(K_\mathrm{I}, K_\mathrm{II}, K_\mathrm{III}, K_\mathrm{D}) = K_\mathrm{c} \tag{8.1}$$

However, it should be noted that the role of K_D is not fully the same as that of $K_\mathrm{I}, K_\mathrm{II}$ and K_III. Many experiments show that the electric energy at failure of a piezoelectric

material is much larger than that in the mechanical fracture. Otherwise the large electric field can produce electric sparking to breakdown the dielectric. As examples Heyer et al. (1998) gave a fracture criterion fitting their measured data in the range $-50 < K_{\mathrm{E}} < 25\ (\mathrm{KVm}^{-1/2})$ for material PET-PIC 151 is

$$K_{\mathrm{I}}(\mathrm{MPam}^{1/2}) = 0.90 - 0.01\,K_{\mathrm{E}}(\mathrm{KVm}^{1/2}) - 0.00002\,K_{\mathrm{E}}^2 \tag{8.2}$$

Fang et al. (2004) gave a fracture criterion fitting their measured data in the range $K_{\mathrm{I}} < 1.5\mathrm{Pam}^{1/2}$ and $-2.5 \times 10^4\mathrm{Vm}^{-1/2} < K_{\mathrm{E}} < 4 \times 10^4\mathrm{Vm}^{-1/2}$ for material PET-5 is

$$K_{\mathrm{I}}(\mathrm{Pam}^{1/2}) + 18.193K_{\mathrm{E}}(\mathrm{Vm}^{-1/2}) - 2.641 \times 10^{-4}K_{\mathrm{E}}^2 = 803505.949 \tag{8.3}$$

8.2.2 Energy Release Rate Criterion

1. *Total Energy Release Rate Criterion*

For linear electroelastic theory, the original energy criterion of the crack extension is

$$G = R, \quad G = -\partial(U - W)/\partial a, \quad R = \mathrm{d}(\gamma_{\mathrm{s}} + \gamma_{\mathrm{i}})/\mathrm{d}a \tag{8.4}$$

where G is the energy release rate, R is crack extension resistance, U is the internal energy, W is the work done by the external force, γ_{s} is the energy to formed a new surface, and γ_{i} is the irreversible work at the crack tip. But we often use the electric enthalpy release rate $\tilde{G}$ as the energy release rate. If the crack tip is selected at the coordinate origin, $\tilde{G}$ is (Suo et al. 1992)

$$\tilde{G} = \lim_{\Delta \to 0} \frac{1}{2\Delta} \times \int_0^{\Delta} \left\{ \sigma_{2j}(r)[u_j^+(\Delta - r) - u_j^-(\Delta - r)] + D_2(r)[\varphi^+(\Delta - r) - \varphi^-(\Delta - r)] \right\} \mathrm{d}r \tag{8.5}$$

where Δ is the crack virtual extension, r is the distance in front of the crack tip on axis x_1 and $\Delta - r$ is the distance behind the crack tip.

The J integral expressed with the electric enthalpy is defined as

$$J = \int_{\Gamma} (gn_1 - \sigma_{ij}n_j u_{i,1} - n_i D_i \varphi_{,1})\,\mathrm{d}l, \quad g = (1/2)(\sigma_{ij}u_{i,j} + D_i\varphi_{,i}) \tag{8.6}$$

where Γ is the integration contour around the crack tip and g is the electric enthalpy density. In the linear- or small-scale yielding case, it can be proved that $\tilde{G} = J$.

For the mode-I fracture tests of the compact tension (CT) specimen, as shown in Sect. 8.1.1, Park and Sun (1995) gave

$$\tilde{G}_{\mathrm{I}} == (\pi a/2)\left[2.29\times10^{-11}\left(\sigma_{33}^{\infty}\right)^2+2.35\times10^{-11}\sigma_{33}^{\infty}E_3^{\infty}-8.78\times10^{-9}\left(E_3^{\infty}\right)^2\right]\mathrm{N/m} \tag{8.7}$$

Equation (8.7) shows that when the contribution of an electric field is larger than that of the mechanical stress, the total energy release rate becomes negative and the crack cannot be extended. For the small stress and large electric field, the electric field always impedes crack propagation. It is contrary to the experimental results.

2. *Mechanical Strain Energy Release Rate Criterion*

Park and Sun (1995) proposed a mechanical strain energy release rate $G_{\mathrm{I}}^{\mathrm{M}}$ criterion for the piezoelectric materials. For the CT test, they got

$$\begin{aligned} G_{\mathrm{I}}^{\mathrm{M}} &= \lim_{\Delta\to0}\frac{1}{2\Delta}\int_0^{\Delta}\left\{\sigma_{33}(r)\left[u_3^{+}(\Delta-r)-u_3^{-}(\Delta-r)\right]\right\} \\ &= (\pi a/2)\left[2.28\times10^{-11}\left(\sigma_{33}^{\infty}\right)^2+1.21\times10^{-11}\sigma_{33}^{\infty}E_3^{\infty}\right]\mathrm{N/m} \end{aligned} \tag{8.8}$$

Equation (8.8) shows that the positive electric field (the direction of the external electric field is consistent with the poling electric field) increases the mechanical strain energy rate and decreases the fracture toughness. The results calculated from this criterion are consistent with that in test, as shown in Fig. 8.13. However, if the stresses are all zeros, Eq. (8.8) shows that the crack cannot be extended; it is also contrary with the experiment. It can be considered that for larger mechanical stress this criterion is well.

3. *Strain Energy Density Factor Criterion*

In elastic fracture mechanics, Sih (1973) proposed the strain energy density factor as the fracture criterion. Zuo and Sih (2000) and Shen and Nishioka (2000) extended this theory to the piezoelectric materials. The strain energy density factor S is defined as

$$S=\lim_{r\to0}r\mathrm{d}U/\mathrm{d}V=\lim_{r\to0}r\mathfrak{A},\quad \mathfrak{A}=\mathrm{d}U/\mathrm{d}V=\sigma_{ij}\varepsilon_{ij}/2+D_iE_i/2 \tag{8.9}$$

where $\mathfrak{A}$ is the strain energy density. The strain energy density factor criterion is assumed:

(a) At the crack tip, the minimum strain energy density $S_{\min}$ happened at $\theta=\theta_0$, $(\partial S/\partial\theta)_{\theta=\theta_0}=0$, and $(\partial^2 S/\partial\theta^2)_{\theta=\theta_0}>0$, where θ is the polar angle. Crack initiation will start at the direction of the max $S_{\min}$.

(b) When max .$S_{\min}$ reaches the critical value S_{c}, the crack begins propagation.

This theory is based on the stress state before crack extension. This theory is not related to the crack virtual extension which is demanded by the energy release rate theory.

According to Eq. (3.222) in general case, the stress asymptotic field near the crack tip for a piezoelectric material with polarized x_3-axis is

$$\begin{aligned}
&\boldsymbol{\Sigma}_1 = -\left(1\Big/\sqrt{2\pi r}\right)\mathrm{Re}\,\boldsymbol{B}\left\langle \mu_\mathrm{k}\Big/\sqrt{\Theta_\mathrm{k}}\right\rangle \boldsymbol{B}^{-1}\boldsymbol{K}, \quad \boldsymbol{\Sigma}_2 = \left(1\Big/\sqrt{2\pi r}\right)\mathrm{Re}\,\boldsymbol{B}\left\langle 1\Big/\sqrt{\Theta_\mathrm{k}}\right\rangle \boldsymbol{B}^{-1}\boldsymbol{K} \\
&\Theta_k = \sqrt{\cos\theta + \mu_k \sin\theta}, \quad K_\mathrm{I} = \sigma_{33}^{\infty}\sqrt{\pi a},\ K_\mathrm{II} = \sigma_{31}^{\infty}\sqrt{\pi a},\ K_\mathrm{III} = \sigma_{32}^{\infty}\sqrt{\pi a},\ K_D = D_3^{\infty}\sqrt{\pi a}
\end{aligned} \tag{8.10}$$

Discuss the plane strain problem in the (x_1, x_3) plane. In this case $E_2 = 0, \varepsilon_{22} = 0$, so $\sigma_{22}\varepsilon_{22} = 0, D_2E_2 = 0$. The strain energy density factor becomes

$$\begin{aligned}
&S = \lim_{r\to 0} r\mathfrak{A} = (1/2)\lim_{r\to 0} r\left[\left(\boldsymbol{\Sigma}_1^{\mathrm{T}}\boldsymbol{\varepsilon}_1 + \boldsymbol{\Sigma}_2^{\mathrm{T}}\boldsymbol{\varepsilon}_2\right) + (\sigma_{31}\varepsilon_{31} + \sigma_{23}\varepsilon_{23})\right] \\
&\boldsymbol{\varepsilon}_1 = (\varepsilon_{11}, \varepsilon_{12}, \varepsilon_{13}, E_1)^{\mathrm{T}}, \quad \boldsymbol{\varepsilon}_2 = (\varepsilon_{21}, \varepsilon_{22}, \varepsilon_{23}, E_2)^{\mathrm{T}}
\end{aligned} \tag{8.11}$$

where generalized strains can be obtained from the constitutive equations, so S can be expressed by the generalized stress intensity factors. Their numerical calculation results show that for the material PZT-4 in the range $-0.6\,(\mathrm{kV/cm}) < E_3 < 0.8\,(\mathrm{kV/cm})$, the theoretical results are consistent with previous experimental results.

8.2.3 Small-Scale Domain Switching Theory

Experiments show that under mechanical and electrical loadings, the intensified generalized stresses near a crack-like flaw lead to domain reorientation. An electric field can rotate the polar direction of a domain by either 180° or 90°, but a stress field rotates it only by 90°. Let the initial poling direction of a domain form an angle ϕ with x_1-axis and the variation of the polarization vector $\Delta\boldsymbol{P}_\mathrm{s}$ and the transformation strain tensor $\Delta\boldsymbol{\varepsilon}_0$ after a 90° rotation of a domain (Fig. 8.8) be, respectively,

$$\Delta\boldsymbol{P}_\mathrm{s} = \sqrt{2}P_\mathrm{s}\begin{bmatrix}\cos(\phi \pm 3\pi/4)\\ \sin(\phi \pm 3\pi/4)\end{bmatrix}, \quad \Delta\boldsymbol{\varepsilon}_0 = \varepsilon_0\begin{bmatrix}-\cos 2\phi & \sin 2\phi\\ \sin 2\phi & \cos 2\phi\end{bmatrix} \tag{8.12}$$

where $\boldsymbol{P}_\mathrm{s}$ is the spontaneous polarization, ε_0 is the spontaneous strain, and $\pm 3\pi/4$ are corresponding to the anticlockwise and clockwise, respectively.

The domain switching plays an important role in the crack extension theory. Zhu and Yang (1997) and Yang and Zhu (1998) proposed a small-scale domain switching theory to qualitatively discuss the fracture toughness variation which is related to the fracture criterion. In their discussion, they assumed outside the switching zone, the interaction between the stress and electric field is neglected and the material is assumed isotropic. In Sect. 5.1.3, the electric field of a permeable elliptic cavity in an electrostrictive material was studied under the assumption that the effect of the stress on the electric field was neglected, so the results in Sect. 5.1.3

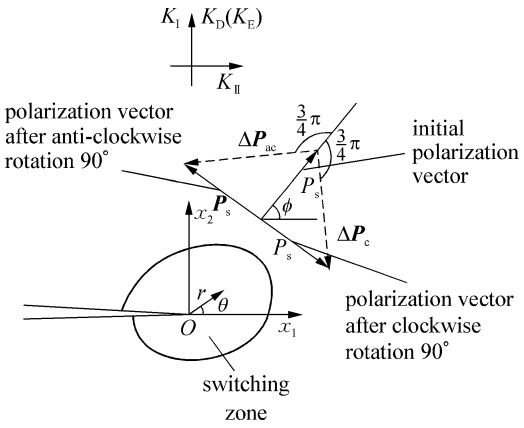

Fig. 8.8 90° switching domain near the crack tip

can be used here. When the external electric field is only E_2^{∞}, the electric asymptotic field near the right end of a narrow ellipse in a local coordinate system with the origin at the focus of the ellipse is (see Eq. (5.34))

$$E_2 \approx E_2^{\infty}\left\{\frac{1}{1+\bar{\delta}}\sqrt{\frac{a}{2r}}\mathrm{e}^{-\mathrm{i}\theta/2}+\frac{1+2\bar{\delta}}{2(1+\bar{\delta})}\right\} \tag{8.13}$$

In Eq. (8.13) the first term is a singular electric field, while the second term is a homogeneous electric field. When $\bar{\delta}$ is small, the singular electric field is dominant, while $\bar{\delta}$ is large, the homogeneous field is dominant. Outside the switching zone, the stress asymptotic field is

$$\sigma_{ij} = \left(K_{\mathrm{app}}\Big/\sqrt{2\pi r}\right)f_{ij}(\theta) \tag{8.14}$$

where K_{app} is the apparent stress intensity factor. The domain switching criterion can approximately expressed as (Hwang et al. 1995)

$$\boldsymbol{\sigma} : \Delta\boldsymbol{\varepsilon} + \boldsymbol{E} : \Delta\boldsymbol{P} \geq 2P_{\mathrm{s}}E_{\mathrm{c}} \tag{8.15}$$

where E_{c} is the coercive electric field. Substitution of Eqs. (8.12), (8.13), and (8.14) into Eq. (8.15) roughly yields the boundary of the switching zone R_0 as:

$$\begin{aligned}
&\sqrt{R_0} = \sqrt{\rho}R(\theta,\beta,\bar{\delta}) > 0; \quad \rho = \frac{1}{8\pi}\left(\frac{K_{\mathrm{app}}\varepsilon_0}{P_{\mathrm{s}}E_{\mathrm{c}}}\right); \quad \beta = \frac{K_{\mathrm{E}}P_{\mathrm{s}}}{K_{\mathrm{app}}\varepsilon_0}, \quad K_{\mathrm{E}} = E^{\infty}\sqrt{\pi a} \\
&R = \left[\frac{\sqrt{2}}{1+\bar{\kappa}}\beta\sin\left(\phi \pm \frac{3\pi}{4} - \frac{\theta}{2}\right) + \sin\theta\,\sin\left(2\phi + \frac{3\theta}{4}\right)\right]\left[1 - \frac{E_2^{\infty}}{\sqrt{2}E_{\mathrm{c}}}\frac{\bar{\delta}}{1+\bar{\delta}}\sin\left(\phi \pm \frac{3\pi}{4}\right)\right]^{-1}
\end{aligned} \tag{8.16}$$

In mono-domain switching case, numerical results showed that when $\bar{\delta} = 10^3$, the uniform electric field is dominant and a positive electric field reduces the

size of the switching zone, while the negative electric field enlarges the size. When $\bar{\delta} = 10^{-3}$, the singular electric field is dominant, and both the positive and negative electric fields enlarge the size of the switching zone.

At the crack tip region, the domain switching occurred. Solved the shape and the size of the switching zone, the toughness increment can be obtained by the transformation theory (Eshelby 1957; McCmeeking and Evans 1982; Budiansky et al. 1983). Zeng and Rajapakse (2001) and Rajapakse and Zeng (2001) discussed the toughness increment by domain switching also. Huang and Kuang (2003) discussed the influence of the switching wake on the facture toughness of ferroelectric materials. The domain switch theory need be improved.

8.3 The Local Energy Release Rate Theory

Usually a piezoelectric material has high mechanical strength, brittleness, and small deformation, but the electric saturation can be occurred under large electric field. Analogous to the Dugdale model in elastoplastic fracture mechanics, Gao et al. (1997) proposed the strip electric saturation model and local energy release rate theory to explain the effect of the electric field on the failure of a crack specimen in piezoelectric material. This model considers that near the crack tip the mechanical deformation is elastic, but the electric field is saturated on a line in front of the crack tip or treats dielectric ceramic as mechanically brittle and electrically ductile (Fig. 8.9). The fracture behavior is determined by the local J integral around the crack tip $x_1 = a$ only and does not enclosed the electric saturation end $x_1 = c$.

1. *Poling Axis Perpendicular to the Crack*

Discuss an infinite plate with a central crack of length $2a$ located on the axis x_1. The polarization x_3-axis is perpendicular to the crack (Fig. 8.9). In order to clearly explain the physical phenomenon, Gao et al. (1997) adopted the following simplified constitutive equation:

$$\begin{Bmatrix} \sigma_{11} \\ \sigma_{22} \\ \sigma_{33} \\ \sigma_{32} \\ \sigma_{31} \\ \sigma_{12} \\ D_1 \\ D_2 \\ D_3 \end{Bmatrix} = \begin{bmatrix} M & * & * & 0 & 0 & 0 & 0 & 0 & e \\ * & M & * & 0 & 0 & 0 & 0 & 0 & e \\ * & * & M & 0 & 0 & 0 & 0 & 0 & -e \\ 0 & 0 & 0 & M & 0 & 0 & 0 & -e & 0 \\ 0 & 0 & 0 & 0 & M & 0 & -e & 0 & 0 \\ 0 & 0 & 0 & 0 & 0 & * & 0 & 0 & 0 \\ 0 & 0 & 0 & 0 & e & 0 & \epsilon & 0 & 0 \\ 0 & 0 & 0 & e & 0 & 0 & 0 & \epsilon & 0 \\ -e & -e & e & 0 & 0 & 0 & 0 & 0 & \epsilon \end{bmatrix} \begin{Bmatrix} \varepsilon_{11} \\ \varepsilon_{22} \\ \varepsilon_{33} \\ 2\varepsilon_{32} \\ 2\varepsilon_{31} \\ 2\varepsilon_{12} \\ E_1 \\ E_2 \\ E_3 \end{Bmatrix} \tag{8.17}$$

where $*$ means that the corresponding material constant does not appear in this model and is omitted. Here the plane strain problem is discussed.

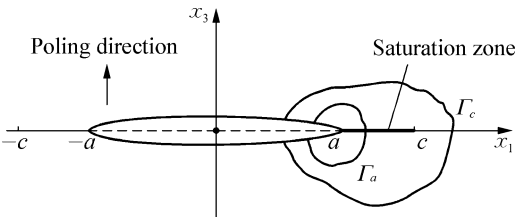

Fig. 8.9 The local J integral model

In Eq. (8.17) there are only three independent material constants M, e, ϵ. Assume the displacement only along x_3 direction, i.e.,

$$u_1 = 0, \quad u_3 = u_3(x_1, x_3), \quad E_i = -\varphi_{,i} \tag{8.18}$$

The equilibrium equation along direction x_1 is satisfied automatically due to $u_1 = 0$, so σ_{11} is not needed. Substitution of Eq. (8.18) into Eq. (8.17) yields

$$\begin{aligned} \sigma_{13} &= Mu_{3,1} + e\varphi_{,1}, \quad \sigma_{33} = Mu_{3,3} + e\varphi_{,3} \\ D_1 &= eu_{3,1} - \epsilon\varphi_{,1}, \quad D_3 = eu_{3,3} - \epsilon\varphi_{,3} \end{aligned} \tag{8.19}$$

Inserting Eq. (8.19) into generalized equilibrium equation $\sigma_{ij,j} = 0$ and $D_{i,i} = 0$ yields

$$\nabla^2 u_3 = 0, \quad \nabla^2 \varphi = 0 \tag{8.20}$$

Introduce complex potentials $U(z)$ and $\Phi(z)$, and let

$$\begin{aligned} &u_3 = \mathrm{Im}[U(z)]; \quad \varphi = \mathrm{Im}[\Phi(z)]; \quad \sigma_{33} + \mathrm{i}\sigma_{31} = MU'(z) + e\Phi'(z) \\ &D_3 + \mathrm{i}D_1 = eU'(z) - \epsilon\,\Phi'(z); \quad E_3 + \mathrm{i}E_1 = -\Phi'(z); \quad z = x_1 + \mathrm{i}x_3 \end{aligned} \tag{8.21}$$

Now discuss the strip electric saturation model. Assume in front of the crack that electric field reaches saturation on $a < x_1 \le c, x_3 = 0$. The boundary conditions are

$$\begin{aligned} &\sigma_{33} + \mathrm{i}\sigma_{31} = \sigma^\infty, \quad E_3 + \mathrm{i}E_1 = E^\infty; \quad \text{when} \quad |z| \to \infty \\ &\sigma_{33} = 0, \quad D_3 = 0; \quad \text{when} \quad |x_1| < a, \quad x_3 = 0 \\ &{u_3}^+ = {u_3}^-, \quad D_3 = D_s; \quad \text{when} \quad a < |x_1| \le c, \quad x_3 = 0 \end{aligned} \tag{8.22}$$

where σ^∞ and E^∞ are real constants. It is noted that σ_{31} cannot be zero in $|x_1| < a$ due to $u_1 = 0$ is assumed. The solution satisfying Eq. (8.22) is

$$\begin{aligned} &U'(z) = \frac{c_1 z}{\sqrt{z^2 - a^2}}, \quad \Phi'(z) = \frac{c_3 z}{\sqrt{z^2 - a^2}} + \frac{c_4 z}{\sqrt{z^2 - c^2}} - \frac{D_s}{\epsilon}\omega(z) \\ &c_1 = \frac{eE^\infty + \sigma^\infty}{M}, \quad c_3 = \frac{e(eE^\infty + \sigma^\infty)}{\epsilon M}, \quad c_4 = -\frac{(e^2 + \epsilon M)E^\infty + e\sigma^\infty}{\epsilon M} \\ &\omega(z) = \frac{2}{\pi}\left[\mathrm{arccot}\left(\frac{a}{z}\sqrt{\frac{z^2 - c^2}{c^2 - a^2}}\right) - \frac{z}{\sqrt{z^2 - c^2}}\arccos\left(\frac{a}{c}\right)\right] \end{aligned} \tag{8.23}$$

where $\omega(z)$ is similar to that in the Dugdale model and has the following behaviors:

$$\begin{aligned} &\omega(z) \to 0, \quad \text{when} \quad z \to \infty; \quad \operatorname{Im}\omega(z) = 0, \quad \text{when} \quad |x_1| > c \\ &\operatorname{Re}\omega(z) = 0, \quad \text{when} \quad |x_1| < a; \quad \operatorname{Re}\omega(z) = 1, \quad \text{when} \quad a < |x_1| < c \end{aligned} \tag{8.24}$$

The condition that the stresses are finite at $|x_1| = c$ yields the size of the saturation zone

$$\rho = c - a = a\sec\left(\frac{\pi}{2}\frac{(e^2 + \epsilon M)E^\infty + e\sigma^\infty}{MD_s}\right) - a = a\sec\left(\frac{\pi}{2}\frac{D^\infty}{D_s}\right) - a \tag{8.25}$$

Near the crack tip the stress field is singular, but the electric field is finite. The singular parts of the stresses are

$$\begin{aligned} &\sigma_{33} = \operatorname{Re}\{MU'(z) + e\Phi'(z)\} = M\frac{c_1(a+r)}{\sqrt{r^2 + 2ra}} + e\left[\frac{c_3(a+r)}{\sqrt{r^2 + 2ra}} - \frac{D_s}{\epsilon}\omega(z)\right] \\ &u_3 = \operatorname{Im}\{U(z)\} = c_1\sqrt{a^2 - x^2}, \quad -a < x < a \end{aligned} \tag{8.26}$$

The local J integral J_a at the crack tip (Fig. 8.9) is:

$$J_a = \int_{\Gamma_a} (gn_1 - \sigma_{ij}n_j u_{j,1} - D_j n_j \varphi_{,1})\,\mathrm{d}s = \frac{\pi a}{2M}\left(1 + \frac{e^2}{\epsilon M}\right)(eE^\infty + \sigma^\infty)^2 \tag{8.27}$$

where $g = (1/2)(\sigma_{ij}\varepsilon_{ij} - D_i E_i)$ is the electric Gibbs free energy. Equation (8.26) can also be obtained by substituting Eq. (8.23) into Eq. (8.5) (Fang et al. 1999). The apparent J integral J_c whose integral path encloses the crack tip and the end of the strip electric saturation is

$$\begin{aligned} J_c &= \int_{\Gamma_c} (gn_1 - \sigma_{ij}n_j u_{j,1} - D_j n_j \varphi_{,1})\mathrm{d}s = J_c + D_s(\varphi^+ - \varphi^-)|_{x_1 = a} \\ &= \frac{\pi a}{2M}\left(1 + \frac{e^2}{\epsilon M}\right)(eE^\infty + \sigma^\infty)^2 - \frac{4D_s a}{\pi\epsilon}\ln\left[\sec\left(\frac{\pi}{2}\frac{(e^2 + \epsilon M)E^\infty + e\sigma^\infty}{MD_s}\right)\right] \\ &\approx \frac{\pi a}{2M}\left[(\sigma^\infty)^2 - (e^2 + \epsilon M)(E^\infty)^2\right] \end{aligned} \tag{8.28}$$

When $\rho \ll a$, the approximate equality is held in Eq. (8.28), which is just the solution for the linear problem. It is obvious that $J_c \neq J_a$. If using $J_c = J_{cr}$ as the fracture criterion, where J_{cr} is the critical value at fracture of J integral, both the positive and negative electric fields decrease J_c, so increases the fracture toughness. If using $J_a = J_{cr}$ as the fracture criterion, the positive electric fields decrease the apparent fracture toughness, while negative electric field increases the apparent fracture toughness. This is consistent with the experiment facts.

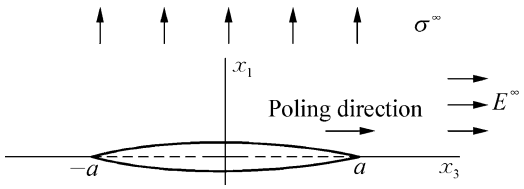

Fig. 8.10 A crack parallel to the poling direction

2. *Poling Axis Parallel to the Crack*

Let the crack be located on the axis x_3 (polarized axis) (Fig. 8.10). Take

$$u_3 = 0, \quad u_1 = u_1(x_1, x_3); \quad D_1 = -\psi_{,3}, \quad D_3 = \psi_{,1} \tag{8.29}$$

In the coordinate system shown in Fig. 8.10, the constitutive equations are

$$\begin{aligned} &\sigma_{13} = \bar{M}u_{1,3} + \bar{e}\psi_{,3}, \quad \sigma_{11} = \bar{M}u_{1,1} + \bar{e}\psi_{,1} \\ &E_3 = \bar{e}u_{1,1} - \bar{\epsilon}\psi_{,1}, \quad E_1 = -\bar{e}u_{1,3} + \bar{\epsilon}\psi_{,3} \\ &\bar{M} = M + e^2/\epsilon, \quad \bar{e} = e/\epsilon, \quad \bar{\epsilon} = -1/\epsilon \end{aligned} \tag{8.30}$$

According to $E_{1,3} = E_{3,1}$ and $\sigma_{11,1} + \sigma_{13,3} = 0$, it can still be derived that u_3 and ψ are all the harmonic functions. Introduce complex potentials $U(z)$ and $\Psi(z)$ and let

$$\begin{aligned} &u_1 = \mathrm{Im}[U(z)], \quad \psi = \mathrm{Im}[\Psi(z)]; \quad \sigma_{11} + \mathrm{i}\sigma_{13} = \bar{M}U'(z) + \bar{e}\Psi'(z) \\ &E_3 - \mathrm{i}E_1 = \bar{e}U'(z) - \bar{\epsilon}\Psi'(z); \quad D_3 - \mathrm{i}D_1 = \Psi'(z); \quad z = x_3 + \mathrm{i}x_1 \end{aligned} \tag{8.31}$$

The solution for a central crack is

$$U'(z) = \frac{\sigma^\infty z}{\bar{M}\sqrt{z^2 - a^2}} + \frac{\bar{e}(\bar{M}E^\infty - \bar{e}\sigma^\infty)}{\bar{M}(\bar{M}\bar{\epsilon} + \bar{e}^2)}, \quad \Psi'(z) = -\frac{\bar{M}E^\infty - \bar{e}\sigma^\infty}{\bar{M}\bar{\epsilon} + \bar{e}^2} \tag{8.32}$$

and

$$J_\mathrm{c} = J_\mathrm{a} = \pi a\sigma^{\infty 2}/2\bar{M} = \pi a\,\epsilon\,\sigma^{\infty 2}/\left[2M(\epsilon M + e^2)\right] \tag{8.33}$$

Equation (8.33) shows that the parallel electric field does not influence the fracture when the poling direction is parallel to the crack. It is also consistent with the experiment facts. If let $x_3 = x, x_1 = y$, the above formulas are identical with that in the paper of Gao et al. (1997).

Wang (2000) and Fulton and Gao (1997) discussed the fracture problem for the strip electric saturation model in a more general situation and pointed out that the local J integral criterion is consistent with the experimental results obtained by Park and Sun in a certain electric field range.

8.4 Failure Criterion of Conductive Cracks with Charge-Free Zone Model

8.4.1 Basic Concept of the Charge-Free Zone

In electronic and electromechanical devices made of piezoelectric ceramics, the embedded soft electrodes are widely used. These soft electrodes may be considered as conducting cracks. When an external electric field is parallel to the conducting crack, the induced charge will be produced on the crack surface in order to make the electric field inside the conducting crack remains zero. The same sign charges will be on the upper and lower surfaces near the crack tip, so the repellent force will open the crack. Zeller and Schneider (1984) proposed a model; they assumed that the charge mobility has a finite value when $E > E_c$, while the charge mobility is zero when $E < E_c$, where E_c is a critical value. Zhang et al. (2003, 2004) based on the above model proposed a charge-free zone (CFZ) model to discuss the failure behavior of conducting crack: When the electric intensity factor at the crack tip reaches a critical value, charges could be emitted from the tip. The emitted charges may form a charge cloud around the tip and shield the external electric field, so form a charge-free zone in front of the tip. Therefore the generalized stress field is singular at the crack tip because there is no electric charge in charge-free zone and the failure criterion can be expressed by the generalized stress intensity factors. The CFZ model is the extension of the dislocation-free model in elastic–plastic fracture mechanics (Ohr 1985; Majumdar and Burns 1983; Kuang et al. 1998).

8.4.2 Interaction of the Crack and a Point Charges in Front of It

Discuss an infinite piezoelectric material polarized along positive x_1-axis with a semi-infinite crack located on the minus x_1-axis subjected to a point electric charge q at z_0 (Fig. 8.11). The crack tip is selected as the origin of the coordinate system. At first discuss the interaction of a single point electric charge in front of the crack tip. Zhang et al. (2004) adopted the simplified constitutive equations shown in Eq. (8.17) with appropriate rearrangement, because the polarized axes are different. In order to discuss the problem qualitatively, it is assumed that

$$u_1 = 0, \quad u_3 = u_3(x_1, x_3) \tag{8.34}$$

$$\begin{aligned} \sigma_{13} &= Mu_{3,1} + e\varphi_{,3}, \quad \sigma_{33} = Mu_{3,3} - e\varphi_{,1} \\ D_1 &= -eu_{3,3} - \epsilon\varphi_{,1}, \quad D_3 = eu_{3,1} - \epsilon\varphi_{,3} \end{aligned} \tag{8.35}$$

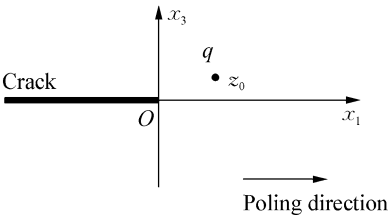

Fig. 8.11 A semi-infinite crack parallel to the poling direction

where u_3 and φ are all harmonic functions, so they can be expressed by complex functions $U(z)$ and $\Phi(z)$:

$$\begin{aligned} &u_3 = \mathrm{Im}[U(z)], \quad \varphi = \mathrm{Im}[\Phi(z)]; \quad z = x_1 + \mathrm{i}x_3 \\ &\sigma_{33} + \mathrm{i}\sigma_{31} = MU'(z) + \mathrm{i}e\Phi'(z); \quad \varepsilon_{33} + \mathrm{i}2\varepsilon_{31} = U'(z) \\ &D_1 - \mathrm{i}D_3 = -eU'(z) + \mathrm{i}\epsilon\Phi'(z); \quad E_3 + \mathrm{i}E_1 = -\Phi'(z) \end{aligned} \tag{8.36}$$

The boundary conditions on a conducting crack surface are

$$\sigma_{33} = 0, \quad E_1 = 0; \quad \text{when} \quad x_1 < 0, \quad x_2 = 0 \tag{8.37}$$

The solution satisfying the boundary conditions is

$$U = 0, \quad \Phi = -\frac{\mathrm{i}q}{2\pi\epsilon}\ln\left(\sqrt{z} - \sqrt{z_0}\right) + \frac{\mathrm{i}q}{2\pi\epsilon}\ln\left(\sqrt{z} - \sqrt{\bar{z}_0}\right) \tag{8.38}$$

Substitution of Eq. (8.38) into Eq. (8.36) yields

$$\begin{aligned} &E_1 - \mathrm{i}E_3 = \mathrm{i}\Phi'(z) = \frac{q}{4\pi\epsilon}\frac{\sqrt{z_0} + \sqrt{\bar{z}_0}}{\sqrt{z}\left[z + \sqrt{z}\left(\sqrt{\bar{z}_0} - \sqrt{z_0}\right) - \sqrt{z_0\bar{z}_0}\right]} \\ &\sigma_{33} + \mathrm{i}\sigma_{31} = e(E_1 - \mathrm{i}E_3); \quad D_1 - \mathrm{i}D_3 = \epsilon(E_1 - \mathrm{i}E_3); \quad \varepsilon_{33} + \mathrm{i}2\varepsilon_{31} = 0 \end{aligned} \tag{8.39}$$

When $z_0 = x_{01}$ is on the x_1-axis, Eq. (8.39) yields

$$\begin{aligned} &E_1 - \mathrm{i}E_3 = \frac{q}{2\pi\epsilon}\frac{\sqrt{x_{01}}}{\sqrt{z}[z - x_{01}]}, \quad K_{\mathrm{E}} = \lim_{z\to 0}\sqrt{2\pi z}(E_1 - \mathrm{i}E_3) = -\frac{q}{\epsilon\sqrt{2\pi\, x_{01}}} \\ &K_\sigma = \lim_{z\to 0}\sqrt{2\pi z}(\sigma_{33} + \mathrm{i}\sigma_{31}) = eK_{\mathrm{E}}, \quad K_{\mathrm{D}} = \lim_{z\to 0}\sqrt{2\pi z}(D_1 - \mathrm{i}D_3) = \epsilon K_{\mathrm{E}} \end{aligned} \tag{8.40}$$

8.4.3 The Condition to Form a Charge-Free Zone

Neglecting the effect of the deformation on the electric field the solution of an infinite material subjected to a point electric charge q is

$$U = 0, \quad \Phi = -\frac{\mathrm{i}q}{2\pi\epsilon}\ln(z - z_0), \quad E_1 - \mathrm{i}E_3 = \frac{q}{2\pi\epsilon}\frac{1}{z - z_0} \tag{8.41}$$

The image field $E_1^{(\mathrm{i})}, E_3^{(\mathrm{i})}$ introduced by the crack is Eq. (8.39) minus (8.41), i.e.,

$$E_1^{(\mathrm{i})} - \mathrm{i}E_3^{(\mathrm{i})} = \frac{q}{2\pi\epsilon}\left[\frac{\sqrt{z_0}+\sqrt{\bar{z}_0}}{2\sqrt{z}\left[z+\sqrt{z}\left(\sqrt{\bar{z}_0}-\sqrt{z_0}\right)-\sqrt{z_0\bar{z}_0}\right]} - \frac{1}{z-z_0}\right] \tag{8.42}$$

When $z_0 = x_{01}$, the image field of a point $z_1 = x_1$ near the crack tip is

$$E_1^{(\mathrm{i})} = \frac{q}{2\pi\epsilon}\left[\frac{\sqrt{x_{01}}}{\sqrt{x_1}\left[x_1 - x_{01}\right]} - \frac{1}{x_1 - x_{01}}\right] = -\frac{q}{2\pi\epsilon}\frac{1}{\sqrt{x_1}\left[\sqrt{x_1}+\sqrt{x_{01}}\right]} \tag{8.43}$$

and image force acted on q is

$$F_{\mathrm{i}} = qE_1^{(\mathrm{i})} = -\frac{q^2}{2\pi\epsilon}\frac{1}{2x_{01}} \tag{8.44}$$

So the image force is always to push the electric charge towards the crack. On the other hand, the external field exerts a driving force F_{a} on the charge. For simplicity discuss a charge, which is on the axis x_{01}. The driving force is given by

$$F_{\mathrm{a}} = K_{\mathrm{E}}q \Big/ \sqrt{2\pi x_{01}} \tag{8.45}$$

where K_{E} is electric field intensity factor produced by the external field. According to Zeller and Schneider's model (1984), when the algebraic sum of the driving force and image force is larger than qE_{c}, the charge will be emitted from the crack tip, or the condition to form a charge-free zone is

$$F_{\mathrm{a}} + F_{\mathrm{i}} \geq qE_{\mathrm{c}}, \quad \frac{K_{\mathrm{E}}q}{\sqrt{2\pi x_{01}}} - \frac{q^2}{4\pi\epsilon}\frac{1}{x_{01}} \geq qE_{\mathrm{c}} \tag{8.46}$$

There are two points $x_1 = a$ and $x_2 = b$ (Fig. 8.12) satisfying Eq. (8.46):

$$\sqrt{x_{1,2}} = \frac{1}{2\sqrt{2\pi}E_{\mathrm{c}}}\left[K_{\mathrm{E}} \pm \left(K_{\mathrm{E}}^2 - \frac{2qE_{\mathrm{c}}}{\epsilon}\right)^{1/2}\right] \tag{8.47}$$

According to Zeller and Schneider's model (1984), a charge moves forward in the region (x_1, x_2) due to $F_{\mathrm{a}} + F_{\mathrm{i}} > qE_{\mathrm{c}}$ and stops at point x_2 due to $F_{\mathrm{a}} + F_{\mathrm{i}} = qE_{\mathrm{c}}$. When more and more charges are emitted from the crack tip, charges will pile up and form a charge trap zone (b, c) followed by the charge-free zone (o, b). It is assumed that b and c are constants.

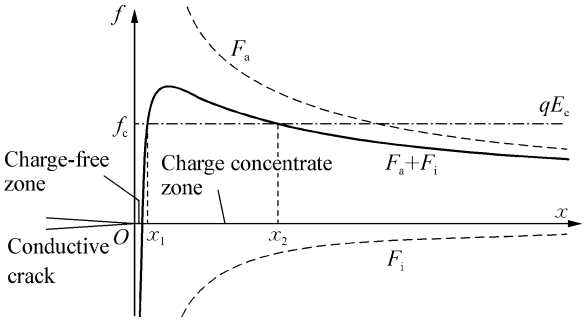

Fig. 8.12 A charge-free zone model

8.4.4 Failure Criterion of Charge-Free Zone Model

Assume the charge density in the charge trap zone is $f(x)$ with $f(b) = f(c) = 0$. The critical electric field is E_c, and the external applied stress intensity factor is $K_E^{(a)}$. Using Eqs. (8.40) and (8.45) the equilibrium condition in the charge trap zone is

$$\frac{K_E^{(a)}}{\sqrt{2\pi x_1}} + \frac{q}{2\pi\epsilon}\int_b^c \frac{f(x_1')\sqrt{x_1'}}{\sqrt{x_1}(x_1 - x_1')}\mathrm{d}x_1' = E_c, \quad b \le x_1 \le c \tag{8.48}$$

In order to guarantee the existence and uniqueness of the solution of $f(x)$ in Eq. (8.48), it must be $f(b) = f(c) = 0$ or (Majumdar and Burns 1983)

$$\int_b^c \frac{E_c\sqrt{x_1'} - K_E^{(a)}/\sqrt{2\pi}}{\sqrt{(c - x_1')(x_1' - b)}}\mathrm{d}x_1' = 0 \tag{8.49}$$

Equation (8.49) yields

$$K_E^{(a)} = 2\sqrt{2\pi c}E_c E(\pi/2, k)/\pi \tag{8.50}$$

where $E(\pi/2, k)$ is the complete elliptic integral of the second kind and $k = \sqrt{1 - b/c}$. The solution of Eq. (8.48) is

$$f(x_1') = -\frac{4\epsilon E_c b\sqrt{x_1'}}{\pi q\sqrt{c}}\frac{\sqrt{c - x_1'}}{x_1'(x_1' - b)}\Pi\left[\frac{\pi}{2}, \frac{x_1'(c - b)}{c(x_1' - b)}, k\right] \tag{8.51}$$

where $\Pi[\pi/2, n^2, k]$ is the complete elliptic integral of the third kind. Using Eq. (8.40) the electric intensity factor produced by the electric charges is

$$\begin{aligned} K_E^{(i)} &= -\sqrt{2\pi}\frac{q}{2\pi\epsilon}\int_b^c \frac{f(x_1')}{\sqrt{x_1'}}\mathrm{d}x_1' = -2\sqrt{\frac{2}{\pi}}E_c\left[\sqrt{c}E\left(\frac{\pi}{2}, k\right) - \sqrt{b}F\left(\frac{\pi}{2}, k\right)\right] = (\Omega - 1)K_E^{(a)} \\ K_\sigma^{(i)} &= e(\Omega - 1)K_E^{(a)}, \quad K_D^{(i)} = \epsilon(\Omega - 1)K_E^{(a)}, \quad \Omega = \sqrt{\frac{b}{c}}F\left(\frac{\pi}{2}, k\right)\Big/E\left(\frac{\pi}{2}, k\right) \end{aligned} \tag{8.52}$$

where $F(\pi/2,k)$ is the complete elliptic integral of the first kind. The local electric field intensity factor at the crack tip is the sum of the applied intensity factor and the intensity factor produced by the charges in the charge trap zone. So we can get

$$\begin{aligned} &K_{\mathrm{E}}=K_{\mathrm{E}}^{(\mathrm{a})}+K_{\mathrm{E}}^{(\mathrm{i})}=\Omega K_{\mathrm{E}}^{(\mathrm{a})}, \quad K_{\mathrm{D}}=K_{\mathrm{D}}^{(\mathrm{a})}+\epsilon(\Omega-1)K_{\mathrm{E}}^{(\mathrm{a})}=\epsilon\left(1+\frac{e^2}{\epsilon M}\right)K_{\mathrm{E}}^{(\mathrm{a})}-\frac{e}{M}K_{\sigma}^{(\mathrm{a})} \\ &K_{\sigma}=K_{\sigma}^{(\mathrm{a})}+e(\Omega-1)K_{\mathrm{E}}^{(\mathrm{a})}, \quad K_{\varepsilon}=K_{\varepsilon}^{(\mathrm{a})}=\left[K_{\sigma}^{(\mathrm{a})}-eK_{\mathrm{E}}^{(\mathrm{a})}\right]/M \end{aligned} \tag{8.53}$$

Using Eq. (8.53) the local J integral J_{a} is obtained:

$$J_{\mathrm{a}}=(1/2)(K_{\sigma}K_{\varepsilon}+K_{\mathrm{D}}K_{\mathrm{E}})=(1/2M)\left(K_{\sigma}^{(\mathrm{a})}-eK_{\mathrm{E}}^{(\mathrm{a})}\right)^2+(\epsilon/2)\left(\Omega K_{\mathrm{E}}^{(\mathrm{a})}\right)^2 \tag{8.54}$$

Assuming J_{cr} is the critical value of J_{a}, Eq. (8.54) yields the fracture criterion:

$$2MJ_{\mathrm{a}}=\left(K_{\sigma}^{(\mathrm{a})}-eK_{\mathrm{E}}^{(\mathrm{a})}\right)^2+\epsilon M\left(\Omega K_{\mathrm{E}}^{(\mathrm{a})}\right)^2=2MJ_{\mathrm{cr}} \tag{8.55}$$

Under purely mechanical loading we can get the critical stress intensity factor $K_{\sigma\mathrm{cr}}$ and under purely electrical loading we can get the critical electric field intensity factor $K_{\mathrm{E\,cr}}$, or

$$\begin{aligned} &K_{\sigma\,\mathrm{cr}}^2=2MJ_{\mathrm{cr}}, \quad \left(\epsilon M\Omega^2+e^2\right)K_{\mathrm{E\,cr}}^2=2MJ_{\mathrm{cr}}; \quad \text{or} \\ &K_{\sigma\,\mathrm{cr}}=\sqrt{2MJ_{\mathrm{cr}}}, \quad K_{\mathrm{E\,cr}}=\pm\sqrt{2MJ_{\mathrm{cr}}/\left(\epsilon M\Omega^2+e^2\right)} \end{aligned} \tag{8.56}$$

where $K_{\mathrm{E\,cr}}$ can be taken as positive or negative value. Using Eq. (8.56), Eq. (8.55) can be rewritten in dimensionless form:

$$\left(\frac{K_{\sigma}^{(\mathrm{a})}}{K_{\sigma\,\mathrm{cr}}}\right)^2\mp\frac{2e}{\left(\epsilon M\Omega^2+e^2\right)^{1/2}}\left(\frac{K_{\sigma}^{(\mathrm{a})}}{K_{\sigma\,\mathrm{cr}}}\right)\left(\frac{K_{\mathrm{E}}^{(\mathrm{a})}}{K_{\mathrm{E\,cr}}}\right)+\left(\frac{K_{\mathrm{E}}^{(\mathrm{a})}}{K_{\mathrm{E\,cr}}}\right)^2=1 \tag{8.57}$$

where the negative sign is for positive electric loading, while the positive sign for negative electric loading. From the derivation process, it is known that the following relation should be held:

$$K_{\sigma\,\mathrm{cr}}^2=\left(\epsilon M\Omega^2+e^2\right)K_{\mathrm{E\,cr}}^2 \tag{8.58}$$

The above relation may not be held for a real material. So from the engineering view, this constraint condition may be abandoned. It may be considered that $K_{\sigma\,\mathrm{cr}}$ and $K_{\mathrm{E\,cr}}$ are two independent experimental parameters and introduce weight

coefficients in Eq. (8.57). If so, the criterion is more like the generalized stress intensity factor criterion Eq. (8.1), but it has certain theoretical foundation. For the problem with general constitutive equations, the results are also consistent with that in experiments (Zhang et al. 2003, 2004).

8.5 Modal Strain Energy Density Factor Theory

8.5.1 *Normalized Generalized Stress and Strain Vectors in Piezoelectric Materials*

As in the elastic case, the first kind of constitutive equations in Eq. (2.83) can be expressed in terms of Voigt vector, i.e.,

$$\begin{aligned}&\boldsymbol{\Gamma} = \boldsymbol{s} \cdot \boldsymbol{\Sigma}\\ &\boldsymbol{\Gamma} = [\varepsilon_x, \varepsilon_y, \varepsilon_z, \gamma_{yz}, \gamma_{zx}, \gamma_{xy}, D_x, D_y, D_z], \quad \boldsymbol{\Sigma} = [\sigma_x, \sigma_y, \sigma_z, \tau_{yz}, \tau_{zx}, \tau_{xy}, E_x, E_y, E_z]\end{aligned} \tag{8.59}$$

where $\gamma_{yz}, \gamma_{zx}, \gamma_{xy}$ are the engineering shear strain. Analogous to Eq. (1.40) the normalized generalized stress vector $\bar{\boldsymbol{\Sigma}}$ and strain vector $\bar{\boldsymbol{\Gamma}}$ in piezoelectric materials are defined as

$$\begin{aligned}&\bar{\boldsymbol{\Gamma}} = \boldsymbol{P}^{-1} \cdot \boldsymbol{\Gamma}, \quad \bar{\boldsymbol{\Sigma}} = \boldsymbol{P} \cdot \boldsymbol{\Sigma}, \quad \boldsymbol{P} = \boldsymbol{P}^{\mathrm{T}} = \mathrm{diag}\left[1\ 1\ 1\ \sqrt{2}\ \sqrt{2}\ \sqrt{2}\ 1\ 1\ 1\right]\\ &\bar{\boldsymbol{\Gamma}} = \bar{\boldsymbol{s}} \cdot \bar{\boldsymbol{\Sigma}}, \quad \bar{\boldsymbol{s}} = \boldsymbol{P}^{-1} \cdot \boldsymbol{s} \cdot \boldsymbol{P}^{-\mathrm{T}}\end{aligned} \tag{8.60}$$

where $\bar{\boldsymbol{s}}$ is the normalized generalized compliance matrix. Let the transform matrix of the coordinate systems ϕ' and ϕ be $\mathbf{Q} = [Q_{kl}]$, $Q_{kl} = \cos(\mathbf{i}_k, \mathbf{i}'_k)$, then

$$\boldsymbol{\Sigma}' = \boldsymbol{A} \cdot \boldsymbol{\Sigma}, \quad \boldsymbol{\Gamma}' = \boldsymbol{B} \cdot \boldsymbol{\Gamma}, \quad \bar{\boldsymbol{\Sigma}}' = \boldsymbol{P} \cdot \boldsymbol{A} \cdot \boldsymbol{P}^{-1} \cdot \bar{\boldsymbol{\Sigma}}, \quad \bar{\boldsymbol{\Gamma}}' = \boldsymbol{P}^{-1} \cdot \boldsymbol{B} \cdot \boldsymbol{P} \cdot \bar{\boldsymbol{\Gamma}} \tag{8.61}$$

where

$$A = \begin{pmatrix} \boldsymbol{A}_{11} & 2\boldsymbol{A}_{12} & 0 \\ \boldsymbol{A}_{21} & \boldsymbol{A}_{22} & 0 \\ 0 & 0 & \boldsymbol{Q} \end{pmatrix}, \quad \boldsymbol{B} = \begin{pmatrix} \boldsymbol{A}_{11} & \boldsymbol{A}_{12} & 0 \\ 2\boldsymbol{A}_{21} & \boldsymbol{A}_{22} & 0 \\ 0 & 0 & \boldsymbol{Q} \end{pmatrix}, \quad \boldsymbol{A}^{\mathrm{T}} = \boldsymbol{B}^{-1} \tag{8.62}$$

where $\boldsymbol{A}_{11}, \boldsymbol{A}_{12}, \boldsymbol{A}_{21}, \boldsymbol{A}_{22}$ are shown in Eq. (1.39). It is easy to show that

$$\begin{aligned}&\boldsymbol{H} = \boldsymbol{P} \cdot \boldsymbol{A} \cdot \boldsymbol{P}^{-1} = \boldsymbol{P}^{-1} \cdot \boldsymbol{B} \cdot \boldsymbol{P}, \quad \boldsymbol{H}^{\mathrm{T}} = \boldsymbol{H}^{-1}\\ &\bar{\boldsymbol{\Sigma}}' = \boldsymbol{H} \cdot \bar{\boldsymbol{\Sigma}}, \quad \bar{\boldsymbol{\Gamma}}' = \boldsymbol{H} \cdot \bar{\boldsymbol{\Gamma}}, \quad \bar{\boldsymbol{\Gamma}}' = \boldsymbol{H} \cdot \bar{\boldsymbol{\Gamma}} = \bar{\boldsymbol{s}}' \cdot \bar{\boldsymbol{\Sigma}}', \quad \bar{\boldsymbol{s}}' = \boldsymbol{H} \cdot \bar{\boldsymbol{s}} \cdot \boldsymbol{H}^{-1}\end{aligned} \tag{8.63}$$

Equation (8.63) shows that $\bar{\boldsymbol{\Sigma}}$ and $\bar{\boldsymbol{\Gamma}}$ are vectors in a nine-dimensional space with the orthogonal coordinate transform tensor $\boldsymbol{H}$.

8.5.2 Eigen Material Constants and Material Modes

Equation (8.60) shows that each component of $\bar{\boldsymbol{\Gamma}}$ are related to all nine components of $\bar{\boldsymbol{\Sigma}}$. Kuang et al. (2003) extended the Kelvin theory (Chen 1984; Ruhlevskii 1984; Arramon et al. 2000) to piezoelectric materials. In material there is a direction $\boldsymbol{M}$, along which $\bar{\boldsymbol{\Gamma}}$ and $\bar{\boldsymbol{\Sigma}}$ are parallel in the nine-dimensional space. The coordinates paralleling to $\boldsymbol{M}$ are called the material principle coordinates. In the material principle coordinates, $\bar{\boldsymbol{\Gamma}}$ is denoted by $\hat{\boldsymbol{\Gamma}}$, $\bar{\boldsymbol{\Sigma}}$ by $\hat{\boldsymbol{\Sigma}}$, and

$$\begin{aligned} &(\bar{\boldsymbol{s}} - \Lambda\mathbf{I}) \cdot \boldsymbol{M} = \mathbf{0}, \quad \hat{\boldsymbol{\Gamma}} = \boldsymbol{\Lambda} \cdot \hat{\boldsymbol{\Sigma}}, \quad \boldsymbol{\Lambda} = \operatorname{diag}[\Lambda_i] = \langle \Lambda_i \rangle \\ &|\bar{\boldsymbol{s}} - \Lambda\mathbf{I}| = \mathbf{0}; \quad \text{or} \quad \left|\boldsymbol{P}^{-1} \cdot \boldsymbol{s} \cdot \boldsymbol{P}^{-\mathrm{T}} - \Lambda\mathbf{I}\right| = \mathbf{0} \end{aligned} \tag{8.64}$$

For the nondegenerate case, Eq. (8.64) has nine different Λ_i, where Λ_i is called ith eigen-compliance and $\boldsymbol{\Lambda}$ is called the eigen-compliance matrix. Usually $\hat{\boldsymbol{s}}$ is real symmetric, so Λ takes real value. For each Λ_i there is an eigenvector or material mode $\boldsymbol{M}_i$ with one arbitrary component. $\boldsymbol{M}_i$ and $\boldsymbol{M}_j$ are orthogonal to each other when $i \neq j$. The normalized orthogonal eigenvectors $\hat{\boldsymbol{M}}$ can be established by

$$\hat{\boldsymbol{M}} = \left[\hat{\boldsymbol{M}}_i\right] = \left[\hat{\boldsymbol{M}}_1, \hat{\boldsymbol{M}}_2, \ldots, \hat{\boldsymbol{M}}_9\right], \quad \hat{\boldsymbol{M}}_i = \boldsymbol{M}_i / |\boldsymbol{M}_i|, \quad \hat{\boldsymbol{M}}\hat{\boldsymbol{M}}^{\mathrm{T}} = \mathbf{I} \tag{8.65}$$

$\hat{\boldsymbol{M}}$ is called the material mode matrix. The space spanning by basis vectors along $\hat{\boldsymbol{M}}$ is called the mode space. Usually the eigen-equation in Eq. (8.64) is degenerate due to the certain symmetry in the real materials, so the number of independent eigenvalues is less than nine, i.e., there are repeated roots in $\boldsymbol{\Lambda}$. However, the eigen-matrix in Eq. (8.64) is semisimple for the real material, so for a multiple root Λ_i, the number of the independent eigenvectors is the same as its multiplicity. Under the coordinate transformation ϕ to ϕ' we have $\hat{\boldsymbol{s}}' = \boldsymbol{H}\hat{\boldsymbol{s}}\boldsymbol{H}^{-1}$, i.e., $\hat{\boldsymbol{s}}'$ and $\hat{\boldsymbol{s}}$ are the similar matrix, so in coordinate systems ϕ and ϕ', the eigen-compliance matrix $\boldsymbol{\Lambda}$ is the same, but the eigenvector changes to $\boldsymbol{M}' = \boldsymbol{H}^{-1}\boldsymbol{M}$.

Analogous to the above discussion, we can also discuss the eigen elastic coefficient matrix $\boldsymbol{\lambda}$:

$$\hat{\boldsymbol{\Sigma}} = \boldsymbol{\lambda} \cdot \hat{\boldsymbol{\Gamma}}, \quad \boldsymbol{\lambda} = \boldsymbol{\Lambda}^{-1} \tag{8.66}$$

8.5.3 Modal Stress, Modal Strain, and Modal Energy Density

Any normalized generalized stress vector $\bar{\boldsymbol{\Sigma}}$ and strain vector $\bar{\boldsymbol{\Gamma}}$ can be decomposed in a modal space:

$$\bar{\boldsymbol{\Sigma}} = \sum_{j=1}^{m} \hat{\boldsymbol{\Sigma}}_j = \sum_{j=1}^{m} \hat{\Sigma}_j \boldsymbol{M}_j, \quad \bar{\boldsymbol{\Gamma}} = \sum_{j=1}^{m} \hat{\boldsymbol{\Gamma}}_j = \sum_{j=1}^{m} \hat{\Gamma}_j \boldsymbol{M}_j \tag{8.67}$$

where $\hat{\boldsymbol{\Sigma}}_j, \hat{\boldsymbol{\Gamma}}_j$ are the j-th modal stress and strain vectors, respectively and $\hat{\Sigma}_j, \hat{\Gamma}_j$ are their norms, respectively. Obviously $\hat{\boldsymbol{\Gamma}}_j = \boldsymbol{\Lambda}_j \hat{\boldsymbol{\Sigma}}_j$. The modal strain energy density $\mathfrak{A}_i$ of ith mode is

$$\mathfrak{A}_i = \hat{\boldsymbol{\Sigma}}_i^{\mathrm{T}} \hat{\boldsymbol{\Sigma}}_i / 2 = \Lambda_i \hat{\boldsymbol{\Sigma}}_i^2 / 2, \quad \text{no sum on } i \tag{8.68}$$

8.5.4 Modal Energy Density Factor (MEDF) Theory

It is believed that the energy possesses the central role in the change of the microstructure and failure. Because the resistance against the change of the microstructure is different in different deformation direction and mechanism, the role of the energy produced in different deformation version and mechanism is different. This fact shows that in the change of the microstructure and failure process, the energy possesses material structure anisotropic behavior. In the small-scale electric saturation case for the self-similarity extended crack, the failure criterion can be determined by the generalized stresses near the tip, so the modal energy density theory can be used. The MEDF failure theory can be expressed as follows:

Assume Λ_{p} is an r-repeated root and its corresponding independent modes are $\boldsymbol{M}_{\mathrm{p}i}, i = 1, 2, \ldots, r$. The subspace spanning by the basic vectors consisted of $\boldsymbol{M}_{\mathrm{p}i}$ is an isotropic subspace for Λ_{p}. Experiences show that the contribution to the failure of each deformation version in this subspace can be considered the same, so $\boldsymbol{M}_{\mathrm{p1}} + \boldsymbol{M}_{\mathrm{p2}} + \cdots + \boldsymbol{M}_{\mathrm{p}r}$ can be considered as one independent mode. Therefore, in the modal strain energy density, the modified number of the independent mode is $N \leq 9$. For the failure problem, the direction (tension or compression) of the generalized stress is also important. Experiments also show that the mechanism of the tension failure is somewhat different with other failure version, so the tension failure criterion should be given alone. Considering these factors, the modal strain energy density theory can be given as

$$\sum_{i=1}^{N} \left(a_i^+ \mathfrak{A}_i^+ + \beta_i a_i^- \mathfrak{A}_i^- \right) = \mathfrak{A}_{\mathrm{cr}}^+ + \beta \mathfrak{A}_{\mathrm{cr}}^- \tag{8.69}$$

where N is the modified number of the independent modes, a_i^+ and a_i^- are the weight coefficients considering the different modal energy, and the superscripts "$+$" and "$-$" express the different direction, β and β_i are the weight coefficients considering deformation direction. For the plastic deformation $a_i^+ = a_i^-$, $\beta = \beta_i = 1$. If all coefficients $a_i^{\pm} = 1, \beta = \beta_i = 1$, Eq. (8.69) is the total energy density criterion. If the generalized stress field is singular with singularity $1/\sqrt{r}$, Eq. (8.69) needs multiply r.

8.5.5 Eigen-Compliances and Material Modes of Some Materials

In practical calculation, Eq. (8.64), $\left(\boldsymbol{P}^{-1}\cdot\boldsymbol{s}\cdot\boldsymbol{P}^{-\mathrm{T}}-\Lambda\mathbf{I}\right)\boldsymbol{M}=\mathbf{0}$, is often used.

1. *Transverse Isotropic Material with Polarized x_3-Axis*

$$\boldsymbol{\Lambda}=\begin{bmatrix} s_{11}-\Lambda & s_{12} & s_{13} & 0 & 0 & 0 & 0 & 0 & d_{31} \\ s_{12} & s_{11}-\Lambda & s_{23} & 0 & 0 & 0 & 0 & 0 & d_{31} \\ s_{13} & s_{23} & s_{33}-\Lambda & 0 & 0 & 0 & 0 & 0 & d_{33} \\ 0 & 0 & 0 & \frac{1}{2}s_{44}-\Lambda & 0 & 0 & 0 & \frac{1}{\sqrt{2}}d_{15} & 0 \\ 0 & 0 & 0 & 0 & \frac{1}{2}s_{44}-\Lambda & 0 & \frac{1}{\sqrt{2}}d_{15} & 0 & 0 \\ 0 & 0 & 0 & 0 & 0 & (s_{11}-s_{12})-\Lambda & 0 & 0 & 0 \\ 0 & 0 & 0 & 0 & \frac{1}{\sqrt{2}}d_{15} & 0 & \epsilon_{11}-\Lambda & 0 & 0 \\ 0 & 0 & 0 & \frac{1}{\sqrt{2}}d_{15} & 0 & 0 & 0 & \epsilon_{11}-\Lambda & 0 \\ d_{31} & d_{31} & d_{33} & 0 & 0 & 0 & 0 & 0 & \epsilon_{33}-\Lambda \end{bmatrix} \tag{8.70}$$

The first and second eigen-compliances are repeated roots $\boldsymbol{\Lambda}_1=\boldsymbol{\Lambda}_2$ and associated with two material modes

$$\begin{aligned} \Lambda_{1,2} &= \left(2\epsilon_{11}+s_{44}+\sqrt{\left(2\epsilon_{11}-s_{44}\right)^2+8d_{15}^2}\right)\Big/4 \\ \boldsymbol{M}_{11}^{\mathrm{T}} &= \left[0,0,0,0,\left(-2\epsilon_{11}+s_{44}+\sqrt{\left(2\epsilon_{11}-s_{44}\right)^2+8d_{15}^2}\right)\Big/2\sqrt{2}d_{15},0,1,0,0\right] \\ \boldsymbol{M}_{12}^{\mathrm{T}} &= \left[0,0,0,\left(-2\epsilon_{11}+s_{44}+\sqrt{\left(2\epsilon_{11}-s_{44}\right)^2+8d_{15}^2}\right)\Big/2\sqrt{2}d_{15},0,00,1,0\right] \end{aligned} \tag{8.71}$$

These two material modes represent the combined version of the shear strains out of the plane (x_1,x_2) and the electric field in the plane (x_1,x_2). The third and fourth eigen-compliances are repeated roots $\boldsymbol{\Lambda}_3=\boldsymbol{\Lambda}_4$ and associated with two material modes

$$\begin{aligned} &\Lambda_{3,4}=s_{11}-s_{12} \\ &\boldsymbol{M}_{31}^{\mathrm{T}}=[-1,1,0,0,0,0,0,0,0,0],\quad \boldsymbol{M}_{32}^{\mathrm{T}}=[0,0,0,0,0,1,0,0,0] \end{aligned} \tag{8.72}$$

These two material modes represent the 2D plane strain in (x_1,x_2) and uncoupled with the electric field. The fifth and sixth eigen-compliances are repeated roots $\boldsymbol{\Lambda}_5=\boldsymbol{\Lambda}_6$ and associated with two material modes

$$\begin{aligned} \Lambda_{5,6} &= \left(2\epsilon_{11}+s_{44}-\sqrt{\left(2\epsilon_{11}-s_{44}\right)^2+8d_{15}^2}\right)\Big/4 \\ \boldsymbol{M}_{51}^{\mathrm{T}} &= \left[0,0,0,0,\left(-2\epsilon_{11}+s_{44}-\sqrt{\left(2\epsilon_{11}-s_{44}\right)^2+8d_{15}^2}\right)\Big/2\sqrt{2}d_{15},0,1,0,0\right] \\ \boldsymbol{M}_{52}^{\mathrm{T}} &= \left[0,0,0,\left(-2\epsilon_{11}+s_{44}-\sqrt{\left(2\epsilon_{11}-s_{44}\right)^2+8d_{15}^2}\right)\Big/2\sqrt{2}d_{15},0,0,0,1,0\right] \end{aligned} \tag{8.73}$$

These two material modes are the counterparts of the first two material modes. The last three eigen-compliances are single roots

$$\begin{aligned}
\Lambda_7 &= \sqrt[3]{-\frac{q}{2}+\sqrt{\left(\frac{q}{2}\right)^2+\left(\frac{p}{3}\right)^3}}+\sqrt[3]{-\frac{q}{2}-\sqrt{\left(\frac{q}{2}\right)^2+\left(\frac{p}{3}\right)^3}}-\frac{a}{3}\\
\Lambda_8 &= \omega\sqrt[3]{-\frac{q}{2}+\sqrt{\left(\frac{q}{2}\right)^2+\left(\frac{p}{3}\right)^3}}+\sqrt[3]{-\frac{q}{2}-\sqrt{\left(\frac{q}{2}\right)^2+\left(\frac{p}{3}\right)^3}}-\frac{a}{3}\\
\Lambda_9 &= \omega^2\sqrt[3]{-\frac{q}{2}+\sqrt{\left(\frac{q}{2}\right)^2+\left(\frac{p}{3}\right)^3}}+\omega\sqrt[3]{-\frac{q}{2}-\sqrt{\left(\frac{q}{2}\right)^2+\left(\frac{p}{3}\right)^3}}-\frac{a}{3}
\end{aligned} \tag{8.74}$$

where

$$\begin{aligned}
&p = b-a^2/3, \quad q = 2a^3/27-ab/3+c, \quad a = -(s_{33}+s_{11}+s_{12}+\epsilon_{33})\\
&b = -2s_{13}^2+s_{33}s_{11}+s_{33}s_{12}+s_{33}\epsilon_{33}+s_{11}\epsilon_{33}+s_{12}\epsilon_{33}-d_{33}^2-2d_{31}^2\\
&c = 2\epsilon_{33}s_{13}^2+(s_{11}+s_{12})\left(d_{33}^2-s_{33}\epsilon_{33}\right)-4s_{13}d_{31}d_{33}+2d_{31}^2s_{33}, \quad \omega = \left(-1+\mathrm{i}\sqrt{3}\right)\Big/2
\end{aligned} \tag{8.75a}$$

and the corresponding material modes are

$$\begin{aligned}
\boldsymbol{M}_7^{\mathrm{T}} &= \left[1,1,\frac{(s_{11}+s_{12}-\Lambda_7)d_{33}-2s_{13}d_{31}}{(s_{33}-\Lambda_7)d_{31}-s_{13}d_{33}},0,0,0,0,0,\frac{(s_{11}+s_{12}-\Lambda_7)d_{33}-2s_{13}d_{31}}{(\epsilon_{33}-\Lambda_7)s_{13}-d_{31}d_{33}}\right]\\
\boldsymbol{M}_8^{\mathrm{T}} &= \left[1,1,\frac{(s_{11}+s_{12}-\Lambda_8)d_{33}-2s_{13}d_{31}}{(s_{33}-\Lambda_8)d_{31}-s_{13}d_{33}},0,0,0,0,0,\frac{(s_{11}+s_{12}-\Lambda_8)d_{33}-2s_{13}d_{31}}{(\epsilon_{33}-\Lambda_8)s_{13}-d_{31}d_{33}}\right]\\
\boldsymbol{M}_9^{\mathrm{T}} &= \left[1,1,\frac{(s_{11}+s_{12}-\Lambda_9)d_{33}-2s_{13}d_{31}}{(s_{33}-\Lambda_9)d_{31}-s_{13}d_{33}},0,0,0,0,0,\frac{(s_{11}+s_{12}-\Lambda_9)d_{33}-2s_{13}d_{31}}{(\epsilon_{33}-\Lambda_9)s_{13}-d_{31}d_{33}}\right]
\end{aligned} \tag{8.75b}$$

These three material modes represent the axial symmetric strains and the electric field out of the plane (x_1, x_2).

2. *Eigen-compliances of a cubic crystal*

$$\begin{aligned}
&\Lambda_1 = s_{11}+2s_{12}, \quad \Lambda_{2,3} = s_{11}-s_{12},\\
&\Lambda_{4,5,6} = \tfrac{1}{2}\epsilon_{11}+\tfrac{1}{4}s_{44}+\tfrac{1}{4}\sqrt{4\,\epsilon_{11}^2-4s_{44}\,\epsilon_{11}+s_{44}^2+8d_{14}^2},\\
&\Lambda_{7,8,9} = \tfrac{1}{2}\epsilon_{11}+\tfrac{1}{4}s_{44}-\tfrac{1}{4}\sqrt{4\epsilon_{11}^2-4s_{44}\,\epsilon_{11}+s_{44}^2+8d_{14}^2}
\end{aligned} \tag{8.76}$$

3. *Eigen-compliances of a hexagonal crystal*

$$
\begin{aligned}
&\Lambda_1 = \epsilon_{33}, \quad \Lambda_{2,3} = s_{11} - s_{12},\\
&\Lambda_4 = \tfrac{1}{2}s_{11} + \tfrac{1}{2}s_{12} + \tfrac{1}{2}s_{33} + \tfrac{1}{2}\sqrt{(-s_{11} - s_{12} - s_{33})^2 - 4\left(-2\epsilon_{13}^2 + s_{11}s_{33} + s_{12}s_{33}\right)},\\
&\Lambda_5 = \tfrac{1}{2}s_{11} + \tfrac{1}{2}s_{12} + \tfrac{1}{2}s_{33} - \tfrac{1}{2}\sqrt{(-s_{11} - s_{12} - s_{33})^2 - 4\left(-2\epsilon_{13}^2 + s_{11}s_{33} + s_{12}s_{33}\right)},\\
&\Lambda_{6,7} = \tfrac{1}{2}\epsilon_{11} + \tfrac{1}{4}s_{44} + \tfrac{1}{4}\sqrt{4\epsilon_{11}^2 - 4s_{44}\,\epsilon_{11} + s_{44}^2 + 8d_{14}^2},\\
&\Lambda_{8,9} = \tfrac{1}{2}\epsilon_{11} + \tfrac{1}{4}s_{44} - \tfrac{1}{4}\sqrt{4\epsilon_{11}^2 - 4s_{44}\,\epsilon_{11} + s_{44}^2 + 8d_{14}^2}
\end{aligned}
\tag{8.77}
$$

4. *Eigen-compliances of a tetragonal crystal*

$$
\begin{aligned}
&\Lambda_1 = \tfrac{1}{2}s_{66}, \quad \Lambda_2 = \epsilon_{33}, \quad \Lambda_3 = s_{11} - s_{12},\\
&\Lambda_4 = \tfrac{1}{2}s_{11} + \tfrac{1}{2}s_{12} + \tfrac{1}{2}s_{33} + \tfrac{1}{2}\sqrt{(-s_{11} - s_{12} - s_{33})^2 - 4\left(-2\epsilon_{13}^2 + s_{11}s_{33} + s_{12}s_{33}\right)},\\
&\Lambda_5 = \tfrac{1}{2}s_{11} + \tfrac{1}{2}s_{12} + \tfrac{1}{2}s_{33} - \tfrac{1}{2}\sqrt{(-s_{11} - s_{12} - s_{33})^2 - 4\left(-2\epsilon_{13}^2 + s_{11}s_{33} + s_{12}s_{33}\right)}\\
&\Lambda_{6,7} = \tfrac{1}{2}\epsilon_{11} + \tfrac{1}{4}s_{44} + \tfrac{1}{4}\sqrt{4\epsilon_{11}^2 - 4s_{44}\epsilon_{11} + s_{44}^2 + 8d_{14}^2},\\
&\Lambda_{8,9} = \tfrac{1}{2}\epsilon_{11} + \tfrac{1}{4}s_{44} - \tfrac{1}{4}\sqrt{4\epsilon_{11}^2 - 4s_{44}\epsilon_{11} + s_{44}^2 + 8d_{14}^2}
\end{aligned}
\tag{8.78}
$$

5. *Eigen-compliances and material modes of an isotropic elastic material*

$$
\begin{aligned}
&\Lambda_1 = s_{11} + 2s_{12} = 1/K, \quad \Lambda_{2,3,4,5,6} = s_{11} - s_{12} = 1/2G,\\
&\boldsymbol{M}_1^{\mathrm{T}} = \left[1\Big/\sqrt{3}, 1\Big/\sqrt{3}, 1\Big/\sqrt{3}, 0, 0, 0\right], \quad \boldsymbol{M}_{21}^{\mathrm{T}} = \left[0, 1\Big/\sqrt{2}, -1\Big/\sqrt{2}, 0, 0, 0\right],\\
&\boldsymbol{M}_{22}^{\mathrm{T}} = \left[\sqrt{2/3}, -\sqrt{1/6}, -\sqrt{1/6}, 0, 0, 0\right], \quad \boldsymbol{M}_{23}^{\mathrm{T}} = [0, 0, 0, 1, 0, 0],\\
&\boldsymbol{M}_{24}^{\mathrm{T}} = [0, 0, 0, 0, 1, 0], \quad \boldsymbol{M}_{25}^{\mathrm{T}} = [0, 0, 0, 0, 0, 1]\\
&\boldsymbol{M}_0^{\mathrm{T}} = \boldsymbol{M}_{21}^{\mathrm{T}} + \boldsymbol{M}_{22}^{\mathrm{T}} + \boldsymbol{M}_{23}^{\mathrm{T}} + \boldsymbol{M}_{24}^{\mathrm{T}} + \boldsymbol{M}_{25}^{\mathrm{T}}\\
&\qquad = \left[\sqrt{2/3}, \sqrt{1/2} - \sqrt{1/6}, -\sqrt{1/2} - \sqrt{1/6}, 1, 1, 1\right]
\end{aligned}
\tag{8.79}
$$

where K and G are the volume compression modulus and shear modulus. In many cases $\boldsymbol{M}_{2i}^{\mathrm{T}}, i = 1 \sim 5$ can be replaced by $\boldsymbol{M}_0^{\mathrm{T}}$. Therefore, for an isotropic elastic material, there are only two different deformation versions: $\boldsymbol{M}_0$ and $\boldsymbol{M}_1$ corresponding to shape and volume changes, respectively. This is the theoretical foundation of the plastic yielding and the failure theory of the elastoplastic materials. The modal energy density theory is more complex, but more rational.

8.5.6 Example

The CT failure test of PZT-4 (Park and Sun 1995) is used as a numerical example to demonstrate the suitability of the MEDF theory. Material constants can be obtained from Sect. 4.4.1 by conversion. The eigen-compliances are

$$\Lambda_{1,2} = 1.3025 \times 10^{-8}\left(\mathrm{m}^2/\mathrm{N}\right), \quad \Lambda_3 = 1.1494 \times 10^{-8}, \quad \Lambda_{4,5} = 1.634 \times 10^{-11},$$
$$\Lambda_6 = 9.9855 \times 10^{-12}, \quad \Lambda_{7,8} = 9.0006 \times 10^{-12}, \quad \Lambda_9 = 3.5413 \times 10^{-12}$$

and the corresponding material modes are

$$\boldsymbol{M}_{11} + \boldsymbol{M}_{12} = [0, 0, 0, -0.02011, 0.02011, 0, 0.7068, -0.7068, 0]^{\mathrm{T}}$$
$$\boldsymbol{M}_3 = [-0.01174, -0.01174, 0.02068, 0, 0, 0, 0, 0, 0.9995]^{\mathrm{T}}$$
$$\boldsymbol{M}_{41} + \boldsymbol{M}_{42} = [-0.5, 0.5, 0, 0, 0, 0.70711, 0, 0, 0]^{\mathrm{T}}$$
$$\boldsymbol{M}_6 = [0.3617, 0.3617, -0.8587, 0, 0, 0, 0, 0, 0.03091]^{\mathrm{T}}$$
$$\boldsymbol{M}_{71} + \boldsymbol{M}_{72} = [0, 0, 0, -0.7068, -0.7068, 0, 0.02011, 0.02011, 0]^{\mathrm{T}}$$
$$\boldsymbol{M}_9 = [0.6075, 0.6075, 0.5118, 0, 0, 0, 0, 0, 0.000918]^{\mathrm{T}}$$

It is seen that the deformation versions are three kinds: $\boldsymbol{M}_{11} + \boldsymbol{M}_{12}$ and $\boldsymbol{M}_{71} + \boldsymbol{M}_{72}$ represent the shear strain out of the plane and the in-plane electric field. In $\boldsymbol{M}_{11} + \boldsymbol{M}_{12}$ the role of the electric field is larger, but in $\boldsymbol{M}_{71} + \boldsymbol{M}_{72}$ the shear strain is larger; $\boldsymbol{M}_{41} + \boldsymbol{M}_{42}$ represents the in-plane stress; $\boldsymbol{M}_3, \boldsymbol{M}_6$ and $\boldsymbol{M}_9$ represent the axial symmetric strain and the electric fields out of the plane.

For the CT specimen in Park and Sun's test (1995), the generalized stress intensity factors are

$$K_{\mathrm{I}} = \sigma_3^{\infty}\sqrt{\pi a}, \quad \sigma_3^{\infty} = 4.4F/tc = 6.16 \times 10^4 F(\mathrm{MPa}); \quad K_{\mathrm{D}} = D_3^{\infty}\sqrt{\pi a}$$

The normalized generalized stress $\bar{\boldsymbol{\Sigma}}$ is

$$\sqrt{r}\bar{\boldsymbol{\Sigma}}$$
$$= \sqrt{a/2}\left[8093F - 1.298E_3^{\infty}, 6922F + 10.2E_3^{\infty}, 6163F, 0, 0, 0, 0, 0, 1440F + 0.974E_3^{\infty}\right]^{\mathrm{T}}$$

where $E_3^{\infty} = D_3^{\infty} \times 10^8 - 1479F$ is obtained from the constitutive equations. Under the above loading the modal energy densities of $\boldsymbol{M}_3, \boldsymbol{M}_{41}, \boldsymbol{M}_{42}$ and $\boldsymbol{M}_6$ are not zero, and they are

$$(r/a)\mathfrak{A}_3 = \left(5 \times 10^{-12}\sigma_3^{\infty 2} + 0.417\sigma_3^{\infty}E_3^{\infty} + 8.69 \times 10^{-9}E_3^{\infty 2}\right)/4$$
$$(r/a)(\mathfrak{A}_{41} + \mathfrak{A}_{42}) = \left(1.47 \times 10^{-13}\sigma_3^{\infty 2} - 1.79 \times 10^{-11}\sigma_3^{\infty}E_3^{\infty} + 5.4 \times 10^{-10}E_3^{\infty 2}\right)/2$$
$$(r/a)\mathfrak{A}_9 = \left(1.4 \times 10^{-11}\sigma_3^{\infty 2} + 7.64 \times 10^{-11}\sigma_3^{\infty}E_3^{\infty} + 1.039 \times 10^{-10}E_3^{\infty 2}\right)/4$$
$$(r/a)\mathfrak{A}_6 = \left(5.44 \times 10^{-15}\sigma_3^{\infty 2} + 1.51 \times 10^{-12}\sigma_3^{\infty}E_3^{\infty} + 1.055 \times 10^{-10}E_3^{\infty 2}\right)/4 \approx 0$$

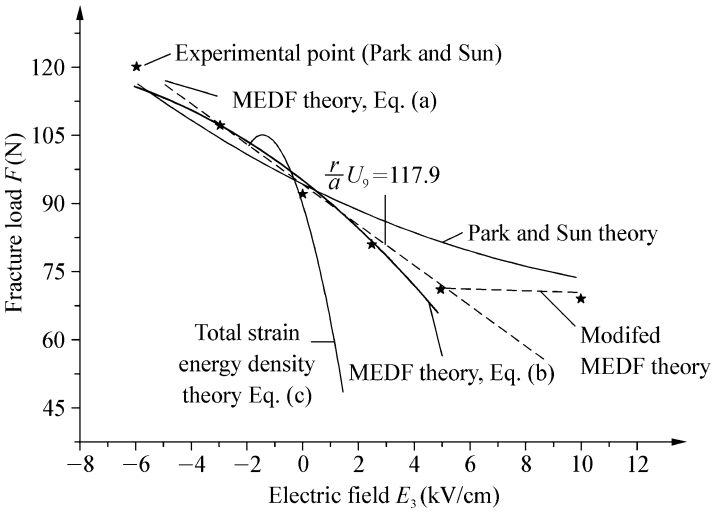

Fig. 8.13 Variations of the fracture load with the electric field

where $\mathfrak{A}_6$ can be neglected. The following criterions (by fitting the test data) are used:

$$(r/a)\mathfrak{A}_9 = \mathfrak{A}_{\text{cr}} \quad \text{or}$$
$$\left(1.4 \times 10^{-11}\sigma_3^{\infty 2} + 7.64 \times 10^{-11}\sigma_3^{\infty}E_3^{\infty} + 1.039 \times 10^{-10}E_3^{\infty 2}\right)/4 = 117.9 \tag{a}$$

$$(r/a)(0.02\mathfrak{A}_3 + 0.05\mathfrak{A}_4 + 0.93\mathfrak{A}_9) = \mathfrak{A}_{\text{cr}}, \quad \text{or}$$
$$\left(1.29 \times 10^{-11}\sigma_3^{\infty 2} + 8.78 \times 10^{-11}\sigma_3^{\infty}E_3^{\infty} + 5.82 \times 10^{-10}E_3^{\infty 2}\right)/4 = 112.9 \tag{b}$$

$$(r/a)(\mathfrak{A}_3 + \mathfrak{A}_4 + \mathfrak{A}_6 + \mathfrak{A}_9) == \mathfrak{A}_{\text{cr}}, \quad \text{or}$$
$$\left(1.95 \times 10^{-11}\sigma_3^{\infty 2} + 4.59 \times 10^{-10}\sigma_3^{\infty}E_3^{\infty} + 9.98 \times 10^{-9}E_3^{\infty 2}\right)/4 = 152.1 \tag{c}$$

Figure 8.13 shows that the theoretical results calculated from Eqs. (a) and (b) are consistent with the results in experiments when $-6\text{kV/cm} < E_3^{\infty} < 6\text{kV/cm}$, but after $E_3 > 6\text{kV/cm}$, the difference is obvious. It can be modified that after $E_3 > 6\text{kV/cm}$, we let $E_3 = 6\text{kV/cm}$ due to saturation. After this modification, the results calculated from Eqs. (a) and (b) are consistent with the results of experiments (Park and Sun 1995) in entire applied loading range. The formula (c) is the same as the total strain energy density factor theory, and the results calculated from it may be appropriated in a narrow loading region only.

8.6 Electric Breakdown of Solid Dielectrics

8.6.1 Energy Criterion

In electric apparatus electric breakdown is often happened. The breakdown is very complicated, here we only qualitatively discuss this problem from the view of the

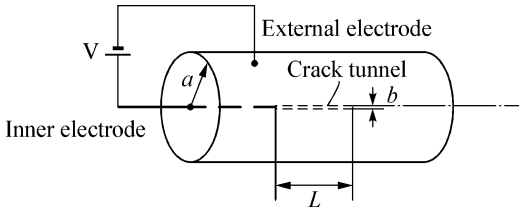

Fig. 8.14 An extending electric tubular channel model

fracture mechanics. The breakdown strength is sensitive to defects, electrodes, and environment. An insulating crack can intensify the field applied perpendicular to the crack, while a conducting crack intensifies the field applied parallel to the crack. Usually dielectric breakdown causes damage along a fine tubular channel. The tubular channel extends forward under external loading. Extending the Griffith theory (1921), Suo (1993) proposed an energy criterion to discuss the electric breakdown in dielectrics. Suo (1993) pointed out that the applied work is partly reversibly stored in the body and partly irreversibly spent to form the thin channel, i.e.,

$$\boldsymbol{f}\cdot \mathrm{d}\boldsymbol{u}+\varphi \mathrm{d}\rho_{\mathrm{e}}=\mathrm{d}\mathfrak{A}+\gamma \mathrm{d}l,\quad \mathrm{d}\mathfrak{A}=\sigma_{ij}\mathrm{d}\varepsilon_{ij}+E_i\mathrm{d}D_i \tag{8.80}$$

where $\boldsymbol{f},\varphi,\rho_{\mathrm{e}},\mathfrak{A}$ are the body force, electric potential, electric charge density, and internal energy density; γ is the work to create a unit length of channel; and $\mathrm{d}l$ is the increment of the channel. On the other hand, the driving force of the channel can be obtained by solving the electroelastic boundary problem, i.e.,

$$\mathrm{d}\Pi=-G\,\mathrm{d}l,\quad G=-\partial\Pi/\partial l,\quad \mathrm{d}\Pi=\mathrm{d}\mathfrak{A}-\boldsymbol{f}\cdot\mathrm{d}\boldsymbol{u}-\varphi\mathrm{d}\rho_{\mathrm{e}} \tag{8.81}$$

where Π is the total potential energy. The energy criterion demands

$$G\geq\gamma \tag{8.82}$$

As an example, Fig. 8.14 shows a slender dielectric cylinder of radius a, inserted a needle-shaped inner electrode and on the cylindrical surface coated metal as the external electrode. The voltage between two electrodes is V. When the voltage reaches a critical value, a conductive channel, radius b and length L, emanates from the needle tip. When $L\gg a$, this problem can be considered as a coaxial transmission line, so the electric potential at a distance r from the center of the channel is

$$\varphi=\varphi_1-\frac{q}{2\pi\epsilon}\ln\frac{r}{b},\quad q=\frac{2\pi\epsilon(\varphi_1-\varphi_2)}{\ln(a/b)} \tag{8.83}$$

where φ_1 and φ_2 are the potentials on the inner channel and external cylindrical surface and q is the electric charge on the channel of a unit length and is constant duo to constant $\varphi_1-\varphi_2$. The work done by the external electric field is $q(\varphi_1-\varphi_2)L$, so we obtain

$$\Pi=-(\varphi_1-\varphi_2)\frac{qL}{2}=-\frac{\pi\epsilon L(\varphi_1-\varphi_2)^2}{\ln(a/b)} \tag{8.84}$$

The energy release rate is

$$\widetilde{G} = -\frac{\partial \Pi}{\partial L} = \frac{\pi \epsilon (\varphi_1 - \varphi_2)^2}{\ln(a/b)} = \frac{\pi \epsilon V^2}{\ln(a/b)} \tag{8.85}$$

According to the energy criterion Eq. (8.82) when $\widetilde{G} \geq \gamma$, the channel will be extended.

8.6.2 J Integral Method

Beom and Kim (2008) discussed the application of J integral to breakdown analysis. From Eq. (2.143), it is known that the following conservation integral is held if the closed integral surface S is not enclosed singular point:

$$\int_V P_{ij,j} \mathrm{d}V = \oint_a \left(g\delta_{ij} - \Sigma_{\alpha j} U_{\alpha,i} \right) n_j \mathrm{d}a = 0 \tag{8.86}$$

where $\boldsymbol{P}$ is the energy-momentum tensor, g is the Gibbs free energy density, and n_i is the outward normal of the surface S. From this theory, it is easy to derive the three-dimensional J integral. For the pure electric loading case we have

$$J_i = \int_S \left(g\delta_{ij} - D_j \varphi_{,i} \right) n_j \mathrm{d}a \tag{8.87}$$

where the surface S with outward normal $\boldsymbol{n}$ is initiated from and stopped on a curve located on the surface defect. Analogous to 2D problem, J integral is equal to the energy release rate. When the channel is fixed, according to the virtual work principle it yields

$$\int_V \delta g \, \mathrm{d}V - \int_{S+S_c} T_i \delta \mathrm{u}_i \, \mathrm{d}a - \int_{S+S_c} D_i n_i \delta\varphi \, \mathrm{d}a = 0 \tag{8.88}$$

When the channel extends with velocity v in a similar version, the variation of the total potential energy Π is

$$\begin{aligned} \delta\Pi &= \delta \int_V g \, \mathrm{d}V - \int_{a_\sigma} T_i \delta u_i \, \mathrm{d}a - \int_{a_D} D_i n_i \delta\varphi \, \mathrm{d}a \\ &= \int_V \delta g \, \mathrm{d}V + \int_{S_c} g v_i \delta t m_i \, \mathrm{d}a + \int_{S_u} T_i \delta u_i \, \mathrm{d}a + \int_{S_\varphi} D_i n_i \delta\varphi \, \mathrm{d}a \\ &= \int_{S_c} g v_i \delta t m_i \, \mathrm{d}a + \int_{S_u} T_i \delta u_i \, \mathrm{d}a + \int_{S_\varphi} D_i m_i \delta\varphi \, \mathrm{d}a \end{aligned} \tag{8.89}$$

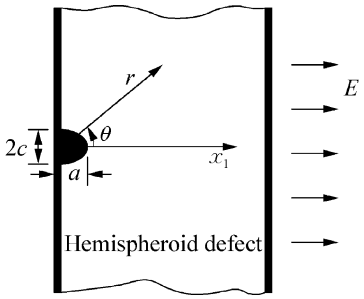

Fig. 8.15 Conducting hemispheroid defect

where $\boldsymbol{m}$ is the external normal of the defect head, so comparing with $\boldsymbol{n}$ in Eq. (8.87) we have $\boldsymbol{m} = -\boldsymbol{n}$. On S_u, u_i is given; on S_φ, φ is given. Using the relation

$$\delta\varphi = -\varphi_{,i} v_i \delta t, \quad \text{on} \quad S_c; \quad v_i = 0, \quad \delta\varphi = 0, \quad \text{on} \quad S - S_c \tag{8.90}$$

So Eq. (8.89) can be written as

$$\delta\Pi/\delta t = \int_{S_c} g v_j m_j \, \mathrm{d}a + \int_{S_c} D_i m_i v_j E_j \, \mathrm{d}a \tag{8.91}$$

Let the channel of length l is located on axis x_1 and extends along x_1, so $v_i = \delta_{i1}\mathrm{d}l/\mathrm{d}t$. Noting the outward normal $\boldsymbol{n} = -\boldsymbol{m}$ of the channel head, so the energy release rate $\tilde{G}$ is

$$\tilde{G} = -\frac{\delta\Pi}{\delta l} = -\frac{1}{\dot{l}}\frac{\delta\Pi}{\delta t} = \int_{S_c} (g n_1 + n_i D_i E_1)\mathrm{d}S \tag{8.92}$$

Equation (8.92) is identical with Eq. (8.87), i.e., $J = \tilde{G}$. Using Eq. (8.87) or (8.92), the effect of the defect shape can be considered.

As an example we discuss a semi-infinite medium with a conductive hemispherical defect of radius $a = c = R$ subjected to a remote uniform electric field E_0 as shown in Fig. 8.15. The solution of a conductive sphere embedded in an infinite dielectric under a remote uniform electric field can be seen in many textbooks. Using the symmetry, the solution of the hemisphere is

$$\varphi = -E_0\left(r - \frac{R^3}{r^3}\right)\cos\theta, \quad E_r = E_0\left[1 + 2\left(\frac{R}{r}\right)^3\right]\cos\theta, \quad E_\theta = -E_0\left[1 - \left(\frac{R}{r}\right)^3\right] \tag{8.93}$$

where r, θ are the sphere coordinates, $r = \sqrt{x_1^2 + x_2^2 + x_3^2}$, and θ is the polar angle measured from the positive x_1-axis. In this case,

$$g = -(1/2)\,\epsilon\left(E_r^2 + E_\theta^2\right), \quad D_r = \epsilon E_r, \quad D_\theta = \epsilon E_\theta \tag{8.94}$$

and

$$J = (9/4)\pi\,\epsilon\, c^2 E_0^2 \tag{8.95}$$

Using the J integral, the electric breakdown can be further discussed.

For a semi-infinite medium with a conductive hemispheroid defect of major semiaxis a and minor semiaxis c subjected to a remote uniform electric field E_0 parallel to x_1-axis. Beom and Kim (2008) adopted the ellipsoid coordinate to solve this problem (Stratton 1941). Finally they got

$$\begin{aligned} J &= \pi\epsilon c^2 E_0^2 H(\lambda) \\ H(\lambda) &= \frac{(1-\lambda^2)\left[(1-\lambda^2)+2\lambda^2\ln\lambda\right]}{2\left[\sqrt{1-\lambda^2}-\lambda\left(\frac{\pi}{2}-\tan^{-1}\frac{\lambda}{\sqrt{1-\lambda^2}}\right)\right]}, \quad \text{when} \quad 0<\lambda=\frac{a}{c}<1 \\ H(\lambda) &= \frac{2\left(\lambda^2-1\right)\left[\left(\lambda^2-1\right)+2\lambda^2\ln\lambda\right]}{2\left[\sqrt{\lambda^2-1}+\lambda\left(\ln\frac{\lambda-\sqrt{\lambda^2-1}}{\lambda+\sqrt{\lambda^2-1}}\right)\right]}, \quad \text{when} \quad \lambda=\frac{a}{c}>1 \end{aligned} \tag{8.96}$$

when $\lambda = a/c \to \infty$, the semi-ellipsoid reduces to a semi-penny-shaped crack and

$$J = \pi\epsilon c^2 E_0^2(\lambda/\ln\lambda), \quad \lambda = a/c \tag{8.97}$$

For more complex cases, the finite element method is an appropriate method.

References

Arramon YP, Mchrabadi MM, Martin DW, Cowin SC (2000) A multi-dimensional anisotropic strength criterion based on Kelvin modes. Int J Solids Struct 37:2915–2935

Beom HG, Kim YH (2008) Application of J integral to breakdown analysis of a dielectric material. Int J Solids Struct 45:6045–6055

Budiansky B, Hutchinson JW, Lambropoulos JC (1983) Continuum theory of dilatant transformation toughening in ceramics. Int J Solids Struct 19:337–355

Chen ST (1984) New concepts of elasticity theory and an application. Acta Mech Sin 16:259–274 (in Chinese)

Eshelby JD (1957) The determination of the elastic field of an ellipsoidal inclusion, and related problems. Proc R Soc Lond A 241:376–396

Fang D, Liu B, Hwang K (1999) Energy analysis on fracture of ferroelectric ceramics. Int J Fract 100:401–408

Fang D, Zhang Z, Soh AK, Lee KL (2004) Fracture criteria of piezoelectric ceramics with defects. Mech Mater 36:917–928

Fu R, Zhang TY (2000) Influences of temperature and electric field on the bending strength of lead zirconate titanate ceramics. Acta Mater 48:1729–1740

Fulton CC, Gao H (1997) Electrical nonlinearity in fracture of piezoelectric ceramics. Appl Mech Rev 50:556–563

Gao HJ, Zhang TY, Tong P (1997) Local and global energy release rates for an electrically yielded crack in a piezoelectric ceramic. J Mech Phys Solids 45:491–510

Griffith AA (1921) The phenomena of rupture and flow in solids. Phil Trans R Soc Lond A 221:163–197

Heyer V, Schneider GA, Balke H, Drescher J, Bahr HA (1998) A fracture criterion for conducting cracks in homogeneously poled PZT-PIC151 ceramics. Acta Mater 46:6615–6622
Huang Z-Y, Kuang Z-B (2003) On the influence of the switching wake on the facture toughness of ferroelectric materials. Smart Mater Struct 12:1017–1022
Hwang SC, Lynch CS, McMeeking RM (1995) Ferroelectric/ferroelastic interactions and a polarization switching model. Acta Metall Mater 43:2073–2084
Jiang LZ, Sun CT (2001) Analysis of indentation cracking in piezoceramics. Int J Solids Struct 38:1903–11918
Kuang Z-B (2011) Theory of electroelasticity. Shanghai Jiaotong University Press, Shanghai (in Chinese)
Kuang Z-B, Gu H-C, Li Z-H (1998) The mechanical behavior of materials. Higher Education Publishing House, Beijing (in Chinese)
Kuang Z-B, Zhou Z-D, Chen Y, Zhao S-X (2003) Eigen-material constants, mode and failure criterion for piezoelectric media. Int J Appl Electromagn Mech 18:235–250
Majumdar BS, Burns SJ (1983) A Griffith crack shielded by a dislocation pile-up. Int J Fract 21:229–240
McCmeeking RM, Evans AG (1982) Mechanics of transformation-toughening in brittle materials. J Am Ceram Soc 65:242–246
Ohr SM (1985) An electron microscope study of crack tip deformation and its impact on the dislocation theory of fracture. Mater Sci Eng 72:1–35
Park S, Sun CT (1995) Fracture criteria for piezoelectric ceramics. J Am Ceram Soc 78:1475–1480
Rajapakse RKND, Zeng X (2001) Toughening of conducting cracks due to domain switching. Acta Mater 49:877–885
Ruhlevskii Y (1984) On Hooke's law. Appl Math Mech 48:420–435 (in Russian); РыхлевскийЯ. ОзаконеГука, прикладнаяматемат и каимехника 48:420–435 (1984)
Shen S-P, Nishioka T (2000) Fracture of piezoelectric materials: energy density criterion. Theor Appl Fract Mech 33:57–65
Sih GC (1973) Some basic problems in fracture mechanics and new concepts. J Eng Fract Mech 5:365–377
Stratton JA (1941) Electromagnetic theory. McGraw-Hill, New York
Suo Z (1993) Models for breakdown-resistant dielectric and ferroelectric ceramics. J Mech Phys Solids 41:1155–1176
Suo Z, Kuo CM, Barnett DM, Willis JR (1992) Fracture mechanics for piezoelectric ceramics. J Mech Phys Solids 40:739–765
Wang T-C (2000) Analysis of strip electric saturation model of crack problem in piezoelectric materials. Int J Solids Struct 37:6031–6049
Wang H, Singh RN (1997) Crack propagation in piezoelectric ceramics: effects of applied electric fields. J Appl Phys 81:7471–7479
Yang W, Zhu T (1998) Switch-toughening of ferroelectrics subjected to electric fields. J Mech Phys Solids 46:291–311
Zeller HR, Schneider WR (1984) Electrofracture mechanics of dielectric aging. J Appl Phys 56:455–459
Zeng X, Rajapakse RKND (2001) Domain switching induced fracture toughness variation in ferroelectrics. Smart Mater Struct 10:203–211
Zhang TY, Wang T, Zhao M (2003) Failure behavior and failure criterion of conductive cracks (deep notches) in thermally depoled PZT-4 ceramics. Acta Mater 51:4881–4895
Zhang TY, Zhao M, Liu G (2004) Failure behavior and failure criterion of conductive cracks (deep notches) in piezoelectric ceramics, I-the charge-free zone model. Acta Mater 52:2013–2024; II-experimental verification. Acta Mater 52:2025–2035 (2004)
Zhu T, Yang W (1997) Toughness variation of ferroelectrics by polarization switch under nonuniform electric field. Acta Mater 45:4695–4702
Zuo J-Z, Sih GC (2000) Energy density theory formulation and interpretation of cracking behavior for piezoelectric ceramics. Theor Appl Fract Mech 34:17–33